·实验研究·

芪黄逐瘀方通过 TNF 信号通路减轻心肌梗死后抑郁的机制研究

李江红[1],孙彤[1],俞鹏[2],沈乐[2],孙伟新[3],陈晓虎[2]
(1. 南京中医药大学第一临床医学院,江苏 南京 210023;2. 南京中医药大学附属医院/江苏省中医院,江苏 南京 210029;3. 南京中医药大学盐城附属中医院/盐城市中医院,江苏 盐城 224000)

摘要:目的 探讨芪黄逐瘀方改善心肌梗死后抑郁的作用机制,重点揭示其对心脑炎症反应的调控作用。**方法** 采用超高效液相色谱-高分辨质谱联用技术(UPLC-Q-TOF/MS)结合网络药理学和分子对接分析芪黄逐瘀方活性成分及干预心肌梗死后抑郁的作用靶点;通过冠状动脉左前降支结扎联合慢性束缚应激建立心肌梗死后抑郁大鼠模型;超声心动图评估心功能,苏木素-伊红(HE)、马松(Masson)染色评估心肌损伤,行为学实验检测抑郁样行为,尼氏(Nissl)染色评估海马神经元损伤,蛋白免疫印迹(Western blot)检测心脏及海马组织中肿瘤坏死因子受体 2(TNFR2)、磷脂酰肌醇-3-羟激酶(PI3K)、磷酸化丝苏氨酸蛋白激酶(p-AKT)、丝苏氨酸蛋白激酶(AKT)、肿瘤坏死因子受体 1(TNFR1)、磷酸化核因子 κB(p-NF-κB)、核因子 κB(NF-κB)的表达;酶联免疫吸附测定法(ELISA)检测血清 IL-6、IL-10 水平,免疫组化技术(IHC)检测 TNFR1、TNFR2 表达;体外实验中,通过大鼠心肌细胞系 H9C2 细胞和大鼠肾上腺嗜铬细胞瘤细胞系高分化 PC12 细胞共培养,给予 TNFR1 抑制剂(H398)和 TNFR2 激动剂(C-6His)干预,通过 Western blot 检测 TNFR2、PI3K、p-AKT、AKT,TNFR1、NF-κB、p-NF-κB 等相关蛋白表达;TUNEL 染色观察细胞凋亡情况;ELISA 法检测细胞上清 IL-6、IL-10 水平。**结果** 网络药理学分析表明,TNF 信号通路是芪黄逐瘀方治疗心肌梗死后抑郁的关键靶点;体内实验证实,芪黄逐瘀方干预可显著改善心肌梗死后抑郁大鼠的心功能、心肌组织与海马神经元结构损伤,并改善其抑郁样行为。分子层面,相较模型组,芪黄逐瘀方高剂量组显著上调心脏和海马组织中的 TNFR2、p-AKT/AKT、IL-10 的表达($P<0.01$),下调 TNFR1、p-NF-κB/NF-κB、IL-6($P<0.01$)水平。体外实验表明,芪黄逐瘀方含药血清在 H9C2 和 PC12 细胞中显著上调 TNFR2、p-AKT/AKT、IL-10($P<0.01$),下调 TNFR1、p-NF-κB/NF-κB、IL-6($P<0.01$)的表达,并显著抑制细胞凋亡($P<0.01$)。此外,联合应用 H398 或 C-6His 的实验进一步证实,芪黄逐瘀方保护及抗炎作用是通过调控 TNFR2/PI3K/AKT 与 TNFR1/NF-κB 通路介导的。**结论** 芪黄逐瘀方通过调节 TNF 通路改善心脑炎症稳态,并改善心肌梗死后抑郁大鼠的心肌损伤和抑郁状态。

关键词: 心肌梗死;抑郁;炎症;芪黄逐瘀方
中图分类号: R285.5 **文献标志码:** A **文章编号:** 1672-0482(2025)09-1148-18
DOI: 10.14148/j.issn.1672-0482.2025.1148
引文格式: 李江红,孙彤,俞鹏,等. 芪黄逐瘀方通过 TNF 信号通路减轻心肌梗死后抑郁的机制研究[J]. 南京中医药大学学报,2025,41(9):1148-1165.

Research on the Mechanism of Qihuang Zhuyu Formula in Alleviating Depression after Myocardial Infarction through the TNF Signaling Pathway

LI Jianghong[1], *SUN Tong*[1], *YU Peng*[2], *SHEN Le*[2], *SUN Weixin*[3], *CHEN Xiaohu*[2]
(1. *The First Clinical Medical College, Nanjing University of Chinese Medicine, Nanjing* 210023, *China*; 2. *Affiliated Hospital of Nanjing University of Chinese Medicine, Jiangsu Province Hospital of Chinese Medicine, Nanjing* 210029, *China*; 3. *Yancheng TCM Hospital Affiliated to Nanjing University of Chinese Medicine, Yancheng TCM Hospital, Yancheng* 224000, *China*)

ABSTRACT: OBJECTIVE To explore the mechanism of action of Qihuang Zhuyu formula (QHZYF) in improving depression after

收稿日期: 2025-06-02
基金项目: 国家自然科学基金面上项目(81973824);国家自然科学基金青年科学基金项目(82205028);江苏省中医药管理局项目(k2021j17-2);江苏省中医院项目(y2021rc06);江苏省中医药科技发展规划项目(QN202118);江苏省中西医结合协会青年科技人才支持项目(JSZXTJ-2024-B05);江苏省青年科技人才支持项目(JSTJ-2024-577)
第一作者: 李江红,女,硕士研究生,E-mail:lijianghong2022@163.com
通信作者: 陈晓虎,男,主任中医师,主要从事心脑血管疾病的防治,E-mail:chenxhdoctor@126.com;
孙伟新,男,副主任中医师,主要从事心血管疾病的中西医防治,E-mail:sunwx@njucm.edu.cn

myocardial infarction (MI), with a focus on revealing its regulatory effect on the inflammatory response of the heart and brain. **METHODS** The active ingredients of QHZYF and the action targets for intervening in depression after MI were analyzed by using ultra-performance liquid chromatography-high-resolution mass spectrometry (UPLC-Q-TOF/MS) combined with network pharmacology and molecular docking. A rat model of depression after MI was established by ligation of the left anterior descending coronary artery combined with chronic restraint stress. Echocardiography was used to evaluate cardiac function, hematoxylin-eosin (HE) and Masson staining were used to evaluate myocardial injury, behavioral tests were used to detect melancholic behaviors, Nissl staining was used to evaluate hippocampal neuron injury. Western blot detection of tumor necrosis factor receptor 2 (TNFR2), phosphatidylinositol-3-kinase (PI3K), phosphorylated seronine protein kinase (p-AKT), seronine protein kinase (AKT), tumor necrosis factor receptor 1 (TNFR1), phosphorylated nuclear factor κB (p-NF-κB), and nuclear factor κB (NF-κB) in cardiac and hippocampal tissues was conducted. The levels of serum IL-6 and IL-10 were detected by enzyme-linked immunosorbent assay (ELISA), and the expression of TNFR1 and TNFR2 was detected by immunohistochemical technique (IHC). *In vitro* experiments, co-culture of rat cardiomyocyte line H9C2 cells and rat adrenal pheochromocytoma cell line with high differentiation PC12 cells was conducted, TNFR1 inhibitor (H398) and TNFR2 agonist (C-6His) were administered for intervention, and the expression of TNFR2, PI3K, p-AKT, AKT, TNFR1, NF-κB, p-NF-κB was detected by Western blot. Observe the apoptosis of cells by TUNEL staining, ELISA was used to detect the levels of IL-6 and IL-10 in the cell supernatant. **RESULTS** Network pharmacological analysis indicates that the TNF signaling pathway was a key target for the treatment of depression after MI with the QHZYF. *In vivo* experiments have confirmed that the intervention of QHZYF could significantly improve the cardiac function, myocardial tissue and hippocampal neuron structure damage of depressed rats after MI, and improve their depression-like behaviors. At the molecular level, the high-dose group of QHZYF significantly upregulated TNFR2, p-AKT/AKT, and IL-10 in cardiac and hippocampal tissues ($P<0.01$), and downregulated TNFR1, p-NF-κB/NF-κB and IL-6 ($P<0.01$). *In vitro* experiments showed that the drug-containing serum of QHZYF significantly upregulated the expression of TNFR2, p-AKT/AKT and IL-10 in H9C2 and PC12 cells ($P<0.01$), downregulated the expression of TNFR1, p-NF-κB/NF-κB and IL-6 ($P<0.01$), and significantly inhibited cell apoptosis ($P<0.01$). Furthermore, experiments on the combined application of H398 or C-6His further confirmed that its protective and anti-inflammatory effects were mediated by regulating the TNFR2/PI3K/AKT and TNFR1/NF-κB pathways. **CONCLUSION** QHZYF improves the homeostasis of heart and brain inflammation by regulating the TNF pathway, and ameliorates myocardial injury and depressive state in depressed rats after MI.

KEYWORDS: myocardial infarction; depression; inflammation; Qihuang Zhuyu formula

Depression significantly increases the risk of cardiovascular events and mortality after a myocardial infarction (MI), making it a critical factor for long-term rehabilitation and prognostic management[1-2]. In a multicentre observational study of 4 062 patients hospitalised for MI, one in five patients reported significant depressive symptoms[3]. However, the impact of depression on patients with MI extends beyond mental health, significantly affecting cardiovascular outcomes. Moreover, patients with post-MI depression have a worse prognosis than those with acute depression, suggesting that post-MI depression may have a unique pathological mechanism[4]. However, significantly improving the depressive state after MI through cardiovascular therapy alone has been proven challenging, while the effect of antidepressant therapy on cardiovascular prognosis is unclear[5]. This complex phenomenon may arise from the bidirectional interaction between the heart and central nervous system[6]. Therefore, exploring the mechanisms underlying post-MI depression could provide important insights for developing novel treatment strategies.

The pathological mechanisms leading to post-MI depression are complex, with inflammatory disorders considered key factors[7-8]. It promotes tissue repair by activating the innate immune system. However, the simultaneous release of numerous inflammatory factors, such as tumour necrosis factor (TNF)-α, can damage the integrity of the blood-brain barrier (BBB), triggering the neuroinflammatory response. The subsequent impact on neuroendocrine regulation, neurotransmitter metabolism, and neuronal remodelling can ultimately lead to depression[9-10]. Indeed, depression and heart failure are associated with significantly higher levels of pro-inflammatory cytokines (i.e., interleukin (IL)-1β, IL-6, TNF-α)[11-12]. Therefore, although local inflammatory responses can be critical to tissue repair after MI, they may also represent a key pathological mechanism that triggers depressive symptoms. Accordingly, inflammatory interventions may offer novel therapeutic strategies to improve the mental well-being of patients after MI.

Selective serotonin reuptake inhibitors (SSRIs) are widely used as antidepressants in clinical practice. However, their effects on cardiovascular prognosis in patients with MI have not been elucidated[13]. Additionally, while non-steroidal anti-inflammatory drugs (NSAIDs) alleviate depressive symptoms, they can increase the risk of cardiovascular diseases[14-15]. These findings underscore the intricate challenges and limitations of current treatments aiming at simultaneously balancing cardiovascular health and alleviating depressive symptoms.

From a traditional Chinese medicine perspective, the relationship between MI and mood disorders is significant. The normal flow of blood and qi is the foundation of vital life functions, which maintains the normal physiological function of the heart and supports mental health. Conversely, blood stasis and qi stagnation, typical symptoms after MI, can lead to chest pain and physical discomfort as well as mental distress and depression[16-18]. Adhering to the therapeutic principle of promoting blood circulation and removing blood stasis, invigorating qi, and strengthening the heart[19], Qihuang Zhuyu formula (QHZYF) has been widely used in the treatment of coronary heart disease and myocardial infarction[20-21]. QHZYF contains five main TCM ingredients: *Astragalus membranaceus Bunge*, *Polygonatum sibiricum*, *Caesalpinia sappan*, *Carthamus tinctorius*, *Hirudo nipponia whitman*. The main chemical components were determined by mass spectrometry, laying the foundation for the study of its pharmacological mechanism.

This study, through network pharmacological screening, explored the potential mechanism of clearing heat and benefiting body fluids in the treatment of depression after MI.

1 Materials

1.1 Experimental animals and cells

Thirty-five male Sprague-Dawley (SD) rats [(150±50) g; 4-5 weeks old] were purchased from SPF (Beijing) Biotechnology [Certificate No. SCXK (Beijing) 2019-0010], with the certificate number of laboratory animal quality (No. 110324241101063225). The rats were raised in the Laboratory Animal Center of Jiangsu Province Hospital of Chinese Medicine [License No. SYXK (Su) 2022-0070], in an SPF

laboratory with a constant temperature of (22±2)℃ and a relative humidity of 55%±5%. The experimental protocol was approved by the Laboratory Animal Ethics Committee of Jiangsu Province Hospital of Chinese Medicine, with the ethics approval number: 2024DW-046-2.

H9C2 cells and PC12 cells were purchased from Noble Biotechnology, with the number: nobcell0074, nobcell0312.

1.2 Preparation of QHZYF

QHZYF contains five main TCM ingredients: *Astragalus membranaceus Bunge* (Huang Qi, HQ), *Polygonatum sibiricum* (Huang Jing, HJ), *Caesalpinia sappan* (Su Mu, SM), *Carthamus tinctorius* (Hong Hua, HH), *Hirudo nipponia whitman* (Shui Zhi, SZ) (Table 1). All herbal ingredients were provided by the Chinese Medicine Preparation Laboratory of Jiangsu Province Hospital of Chinese Medicine and were verified by two Chinese medicine pharmacists. The ratio was 30∶15∶10∶10∶6. All herbs were soaked in 2 L of double-steamed water for 30 min and boiled for 30 min. The filtrate was collected, and the residue was boiled again in 2 L of double-steamed water for 30 min. After combining the filtrate from the two decoctions, the solution was concentrated to 1.05 g·mL^{-1} under reduced pressure (pressure range: −0.04 to −0.01 MPa, temperature: 60 ℃). Subsequently, the supernatant was centrifuged at 6 000 r·min^{-1} and a flow rate of 4-6 L·min^{-1} to obtain QHZYF.

Table 1　Details of QHZYF

Formula components	Traditional Chinese name	Scientific name	Component family	Weight in QHZYF/g
Milkvetch Root	Huang Qi	*Astragalus membranaceus Bunge*	Leguminosae	30
Manyflower Solomonseal Rhizome	Huang Jing	*Polygonatum sibiricum*	Asteraceae	15
Sappan Wood	Su Mu	*Caesalpinia sappan*	Leguminosae	10
Safflower	Hong Hua	*Carthamus tinctorius*	Asparagaceae	10
Leech	Shui zhi	*Hirudo nipponia whitman*	Hirudinidae	6

1.3 Reagents

Isoflurane (Ruiwode Life Science and Technology Co., Ltd, R510-22-10); Protein lysate (RIPA, Shanghai Beyotime Biotechnology Co., Ltd, P0038); phenylmethyl sulfonyl fluoride (PMSF, Shanghai Beyotime Biotechnology Co., Ltd, ST2573); BCA protein concentration assay kit (Shanghai Beyotime Biotechnology Co., Ltd, P0009); CCK-8 Cell Counting Kit (Nanjing Vazyme Biotechnology Co., Ltd, A311-01); TUNEL staining kit (Nanjing Vazyme Biotechnology Co., Ltd, A112-03); ECL Luminescence Kit (Biosharp Biological Reagent Co., Ltd, BL520A); Antibodies: Tumor necrosis factor receptor 2 (TNFR2, Wuhan Proteintech Co., Ltd, 19272-1-AP), Phosphorylated seronine protein kinase (p-AKT, Wuhan Proteintech Co., Ltd, 66444-1-Ig), phosphatidylinositol-3-kinase (PI3K, Wuhan Proteintech Co., Ltd, 20584-1-AP), seronine protein kinase (AKT, Wuhan Proteintech Co., Ltd, 10176-2-AP), tumor necrosis factor receptor 1 (TNFR1, Wuhan Proteintech Co., Ltd, 21574-1-AP), phosphorylated nuclear factor κB (p-NF-κB, Wuhan Proteintech Co., Ltd, 82335-1-RR), nuclear factor κB (NF-κB, Wuhan Proteintech Co., Ltd, 80979-1-RR), β-actin (β-actin, Wuhan Proteintech Co., Ltd, 66009-1-Ig), TNFR1 inhibitor (H398, USA, Hycult Biotech Co., Ltd, 38577M0724); TNFR1 agonist (C-6His, Suzhou, novoprotein Co., Ltd, P20333); Fetal bovine serum (Suzhou Excell Biotechnology Co., Ltd, FCS500); Cell culture medium (Wuhan Procella Biotechnology Co., Ltd, PM150115); VisuTrack (Xin Ruan, Shanghai, China).

1.4 Instrument

Nikon upright fluorescence microscope (Nikon Corporation, Japan); Bio-rad electrophoresis apparatus (USA); Bio-rad gel analysis system (USA); Waters Acquity UPLC Class I ultra-performance liquid chromatograph and Waters SYNAPT G2-S Q-TOF/MS high-resolution mass spectrometer (Waters, USA); ventilators (HX-300S; Chengdu Technology Software Co, LTD, Chengdu, China); ultramicrotome (Reichert Ultracut E; Leica, Wetzlar, Germany); transmission electron microscopy (TEM, JEM-1010; Olympus Corp).

2　Methods

2.1 Identification of active ingredients by Ultra High performance liquid chromatography-high resolution mass spectrometry (UPLC-Q-TOF/MS)

QHZYF solution (1 mL; 1 g·mL^{-1}) was diluted in 10 mL of ultrapure water, vortexed for 1 min, and ultrasonicated in an ice bath for 10 min. Subsequently, the sample was treated with a three-fold methanol solution, vortexed for 1 min, and centrifuged at 13 000 r·min^{-1} for 15 min. The supernatant was separated on a Waters Acquity UPLC BEH C18 column (2.1 mm×100 mm, 1.7 μm) under the following conditions: flow rate, 0.3 mL·min^{-1}; column temperature, 40 ℃; sample size, 5 μL; mobile phase A, 0.1% aqueous formic acid solution; mobile phase B, 0.1% formic acetonitrile solution. The gradient elution procedure was as follows: 0-9 min, 95-60% A; 9-19 min, 60-10% A; 19-25 min, 10-5% A; 25-27 min, 5% A; 27-28 min, 5-95% A; 28-30 min, 95% A.

Mass spectrometry was performed using an electrospray ionisation (ESI) source operating in the positive and negative ion modes under the following conditions: auxilliary spray and gas, high-purity nitrogen; dry gas flow rate, 10 mL·min^{-1}; dry temperature, 120 ℃; atomised gas pressure, 310 kPa; solvent nitrogen flow rate, 900 L·h^{-1}; cone gas purge flow rate, 50 L·h^{-1}; capillary voltage, 500 V; cone voltage, 40 V; impact energy range, 40-65 eV; scanning range, 50-1 500 Da; mass range, *m/z* 50-1 200. A Waters Acquity UPLC Class I ultra-high-performance liquid chromatograph and Waters SYNAPT G2-S Q-TOF/MS high-resolution mass spectrometer were employed.

2.2 Network pharmacology and bioinformatics analysis

The compounds in each herb in QHZYF were identified and screened from the Traditional Chinese Medicine (TCM) database and related literature. The herbal compound sources of HQ, HJ, HH, SM, and SZ included the BATMAN database (http://bionet.ncpsb.org.cn/batman-tcm/), Traditional Chinese Medicine Pharmacology and Analysis Platform (https://old.tcmsp-e.com/), and Herb database (http://herb.ac.cn/). The target names were normalised using the UniProt database (http://www.uniprot.org/). Keywords such as "MI", "myocardial infarction", and "depression" were used to retrieve disease-associated targets from GeneCards (https://www.genecards.org/), Online Mendelian Inheritance in Man (OMIM; https://omim.org/), and Comparative Toxicogenomics Database (CTD;

https://ctdbase.org/). After organising the screening results, duplicate entries were removed, and a Venn diagram was generated to visualise the drug-disease target intersection. Intersection data were imported into the STRING platform for protein-protein interaction (PPI) network analysis and topological analysis using Cytoscape 3.9.1 software; the MCODE plug-in was used to identify core targets in the PPI network. Finally, the DAVID database (https://david.ncifcrf.gov/) was used for target gene enrichment and Kyoto Encyclopedia of Genes and Genomes (KEGG)/Gene Ontology (GO) functional analysis. Pathways with a significance level of $P<0.05$ were visualised.

2.3 Molecular docking verification

By screening PPI core targets and KEGG and GO analyses, TNFR1 and TNFR2 were identified as core targets; potentially associated compounds in QHZYF were screened. The three-dimensional structures of the protein receptors were obtained from the PDB database (http://www.rcsb.org/); the two-dimensional structures of key compounds from QHZYF were extracted from the PubChem database (https://pubchem.ncbi.nlm.nih.gov/) and transformed into three-dimensional structures using Chem3D software. After removing the water molecules and small molecular ligands using PyMOL software, the target protein receptors were protonated using AutoDockTools 1.5.6. Additionally, AutoDock Vina was employed to simulate molecular docking and calculate binding energies. The predicted 3D binding sites were visualised using PyMOL software. An affinity of < -5.0 kcal · mol^{-1} indicated a significant interaction between the protein receptor and compound ligand.

2.4 Construction of depression rat model after MI

After completing the behavioural tests and excluding rats showing signs of depression, thirty-five SD rats were randomly divided into five groups: control group (Normal), sham operation group (Sham), model group (Model), low-dose (3.55 g · kg^{-1} · day^{-1}) QHZYF group (Model+QHZYF-L), and high-dose (7.1 g · kg^{-1} · day^{-1}) QHZYF group (Model+QHZYF-H). The concentration of the stock QHZYF solution was 1 g · mL^{-1}. The dosage for animal administration was determined based on the body surface area conversion method, referencing the clinical dosage for adults of 71 grams crude drug per person per day[21-22]. In clinical practice, current international guidelines do not provide clear recommendations for the specific treatment of post-MI depression, positive control was not used in this study.

To avoid postoperative intestinal obstruction, the rats in the model group were deprived of water the day before modelling. During surgery, ventilators were used for isoflurane anaesthesia and respiratory maintenance through oral tube intubation. The respiratory rate was set at 60 times · min^{-1}, the tidal volume was 1.5-2 mL, and the suction/breathing ratio was 1∶1. The rats were fixed in the supine position, and the left anterior chest was opened in the second intercostal space. The 1.5 cm incision was made, and the skin and muscle layers were separated. The posterior fascia was bluntly separated using eye forceps. After using an eyelid retractor to separate the pectoralis major and serratus anterior, the thorax was gently pierced with haemostatic forceps and the intercostal space was gradually opened to tear the pericardium. The left auricle was lifted using non-toothed tweezers to expose the aortic root, and the coronary vein accompanying the left anterior descending artery (LAD) was exposed. The LAD was blocked by ligating a small bundle of myocardium with a 6-0 suture at a depth of 2 mm and width of 3 mm below the conus of the right ventricular pulmonary artery and left atrial appendage. After successful ligation, the apex of the heart was gently exposed using eye forceps to confirm that it had become pale or grey. The rats in the sham operation group underwent threading under the LAD without ligation. After the operation, the chest cavity was rinsed with penicillin solution and closed layer-by-layer with 4-0 silk sutures once stable blood flow was achieved. Mechanical ventilation was maintained for 5 min after surgery, and the ventilator was gradually removed. Rats were transferred to a hotplate resuscitation device in a lateral position to avoid asphyxia. Rats in the sham, model, low-dose, and high-dose QHZYF groups were confined to an appropriately sized scaffold under fixed pressure, starting on Day 3 after surgery and in a container with restricted movement for 4 h daily to simulate bed rest conditions for one month after MI[23].

2.5 Echocardiographic measurements

The high-frequency ultrasound system Vevo2100 was used to evaluate cardiac function and structure in rats. Rats were anaesthetised with 5% isoflurane using a ventilation device. The fur on the left chest was carefully removed to facilitate contact with the ultrasound probe. Two-dimensional echocardiographic measurements were performed to track and measure the left ventricular end-diastolic diameter (LVIDd) and end-systolic diameter (LVIDs) from the M-mode images. Additionally, the left ventricular ejection fraction (LVEF) and fractional systolic fraction (LVFS) were calculated to quantify cardiac function parameters.

2.6 Behavioural tests

2.6.1 Forced swimming test　A transparent cylindrical tank (diameter: 20-30 cm, height: 40-50 cm) was filled with water (25±1)℃ to a 20-30 cm in depth. The experiment was conducted over two days. On the first day, the rats were placed in the tank and allowed to swim for 15 min to acclimatise to the environment. The formal test was repeated the following day, lasting 5 min, using VisuTrack.

2.6.2 Open field test　A square-enclosed open field was divided into centre and edge areas. To ensure the test site was clean and odourless, it was wiped with 75% alcohol before each experiment and allowed to air-dry. The animals were gently placed in the centre of an open field, and their activity in the open field was recorded for 5 min, VisuTrack software was used for analysis.

2.6.3 Sucrose preference test (SPT)　Before starting the test, the animals were provided two water bottles, one containing pure water and the other a 2% sucrose solution, to ensure they were familiar with the experimental setup. The animals were fasted and water-restricted for 12 h before testing. During the experiment, two water bottles of a known volume were placed in each animal's cage for 30 min. The amount of liquid remaining in the two water bottles was recorded after 30 min, and the consumption of sugar and pure water was calculated.

2.7 Histopathological staining

The heart and brain tissues were fixed with 10% paraformaldehyde, embedded in paraffin, and sectioned into 4 μm slices. Cardiac sections were stained with hematoxylin eosin (HE) and Masson's trichrome to evaluate the pathological changes and degree of myocardial fibrosis. Nissl staining was used to observe morphological changes in the hippocampal neurons and to assess damage.

2.8 Ultrastructural damage assessment

The heart and hippocampal tissues of rats were cut into 1 mm^3 pieces and sequentially fixed in 4% glutaraldehyde and 4% osmium tetroxide solutions for 24 h. Samples were dehydrated in acetone, embedded in resin, and sectioned into ultrathin slices using an ultramicrotome. The sections were stained with 1% uranyl acetate and 0.2% lead citrate to enhance

contrast. Finally, transmission electron microscopy was used to acquire images for ultrastructural analysis.

2.9 Western blot

Proteins were extracted from the left ventricular tissue, hippocampus and cells and separated by sodium dodecyl-sulphate polyacrylamide gel electrophoresis (SDS-PAGE). The isolated proteins were transferred to a polyvinylidene fluoride (PVDF) membrane using an electrotransfer apparatus and blocked with 5% bovine serum albumin at room temperature for 1 h to prevent nonspecific binding. The membrane was incubated with the appropriate primary antibodies at 4 ℃ overnight: TNFR1 (1∶1 000), TNFR2 (1∶500), p-AKT (1∶1 500), PI3K (1∶1 000), AKT (1∶1 000), p-NF-κB (1∶1 000), NF-κB (1∶1 000), and β-actin (1∶10 000). Subsequently, after washing the membrane with Tris-buffered saline (TBST), a secondary antibody (1∶10 000) was added and incubated at room temperature for 1 h. An ECL kit was used for chemiluminescence detection, and a Bio-Rad imaging system was used to record and analyse the Western blot results.

2.10 Enzyme-linked immunosorbent assay (ELISA)

The concentrations of IL-6 and IL-10 in the serum and cell culture supernatants were determined by sandwich ELISA according with the manufacturer's instructions. Finally, measure the absorbance at the specified wavelength and calculate the sample concentration.

2.11 Immunohistochemistry

After the heart and brain tissues were fixed with paraformaldehyde, they were embedded in paraffin, sectioned, dewaxed, rehydrated, permeabilised, and subjected to antigen retrieval. Non-specific binding was blocked with 5% BSA at room temperature for 1 h. Subsequently, TNFR1 and TNFR2 antibodies were diluted and incubated at 4 ℃ overnight, according to the recommended dilution ratios. The next day, samples were incubated with secondary antibodies at room temperature for 1 h. Finally, diaminobenzidine (DAB) colour development was performed using a DAB solution, and haematoxylin was used for nuclear staining.

2.12 Cell culture and modelling

H9C2 (rat cardiac myoblasts) cells and PC12 (rat highly differentiated pheochromocytoma 12) cells were cultured at 37 ℃ and 5% CO_2 in Dulbecco's modified eagle medium supplemented with foetal calf serum; media was replaced every two days. Prior to the experiment, H9C2 and PC12 cells were pre-cultured in 12-well plates for 24 h. H9C2 cells were cultured in an anoxic environment (4% CO_2, 1% O_2, and 94% N_2) for 24 h, whereas PC12 cells were maintained in a normoxic environment. Subsequently, the cells were co-cultured under normal conditions for 24 h to establish a cell model of post-MI depression.

2.13 Preparation of medicated serum

SD male rats (8-10 weeks, 300±50 g) were randomly assigned to the control and QHZYF-treated (7.1 g·kg^{-1}·day^{-1}) groups (n=15 per group). The control group received the corresponding dose of normal saline daily. Both groups were administered via intragastric gavage for seven consecutive days. 2 h after the last dose, the rats were anaesthetised with isoflurane and blood was collected from the abdominal aorta. Sera was separated from blood by centrifugation, heat-inactivated, sterilised through a 0.22 μm microporous filter, and stored at −80 ℃ for further analysis.

2.14 CCK-8 cell proliferation assay

The activities of H9C2 and PC12 cells were evaluated using the CCK-8 assay kit according to the manufacturer's instructions. H9C2 and PC12 cells were seeded in 96-well plates (4×10^3 cells·well^{-1}) and incubated for 24 h. Subsequently, CCK-8 reagent was added and incubated at 37 ℃ for 4 h. Absorbance was measured at 450 nm using an automated microplate reader to assess cell activity.

2.15 TUNEL/DAPI immunofluorescence analysis of apoptosis

Apoptosis was assessed using a terminal deoxynucleotidyl transferase dUTP nick end labelling (TUNEL) staining fluorescence assay kit; the nuclei were quantified using 4′6-diamidino-2-phenylindole (DAPI) staining. TUNEL-positive cells were observed under a fluorescence microscopeat 200× magnification. The areas of TUNEL and DAPI positive staining were quantitatively analysed using Image J software to assess the apoptosis rates and total cell counts.

2.16 Statistical analysis

All data analyses were performed using the GraphPad Prism 10 software. Data are expressed as $\bar{x}\pm s$. The Student's t-test was used to compare two independent groups, whereas an one-way analysis of variance (ANOVA) was performed to compare three or more groups. Statistical significance was set at $P<0.05$.

3 Results

3.1 Potential compounds of QHZYF for predicting depression after MI

Through a database and literature search, all components of QHZYF were identified and compared with the experimental UPLC-Q-TOF/MS results. Details of the UPLC-Q-TOF/MS identification are provided in the research group's prior publication[21]. The assumed targets of these core compounds were compared with the disease-related core targets obtained from the GeneCards, OMIM, and CTD databases. Through intersection analysis of the Venn diagram, 103 candidate targets were selected and uploaded to the STRING 11.0 database for PPI network analysis. A network topology analysis was performed on all identified targets to construct an interactive network (Fig. 1). Subsequently, the STRING analysis results were imported into the Cytoscape 3.9.1 software, and the MCODE plug-in was used for further analysis of network centrality (Fig. 2). The identified core proteins were imported into the DAVID database for GO (Fig. 3) and KEGG (Fig. 4) functional enrichment analyses. AKT1, IL-1β, IL-6, and TNF were identified as the core targets of QHZYF in the treatment of post-MI depression, with key pathways including the TNF signalling pathway.

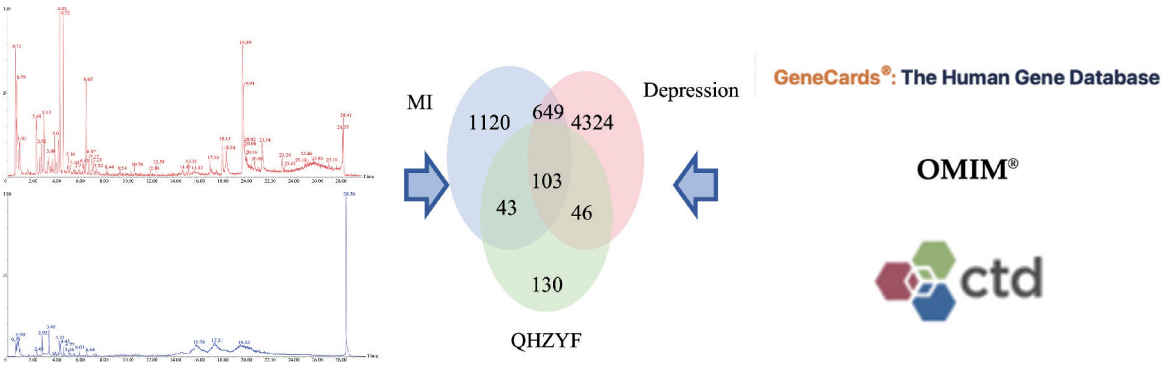

Fig. 1　Venn diagram of the intersection between main targets of related compounds

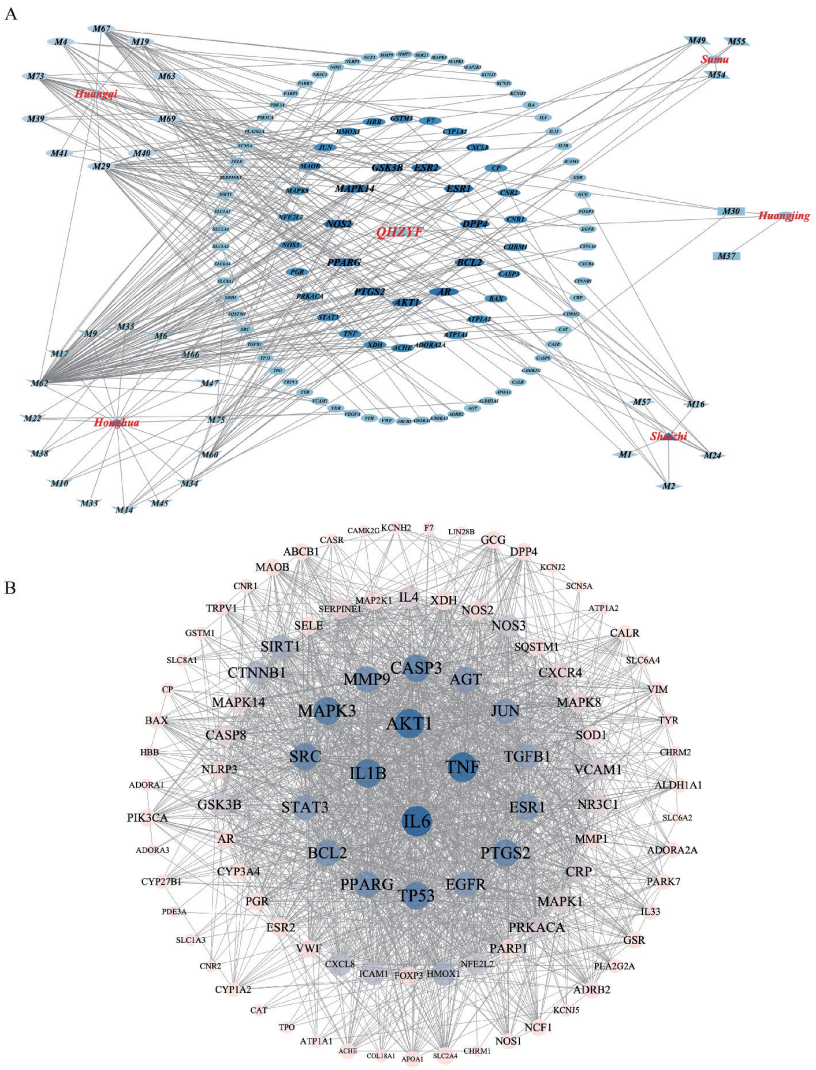

Note: A. Traditional Chinese medicine-component-target network; B. Diagram of the core target network. Larger points represent higher-level associations. Network core target analysis was performed through network centrality analysis.

Fig. 2　PPI network maps

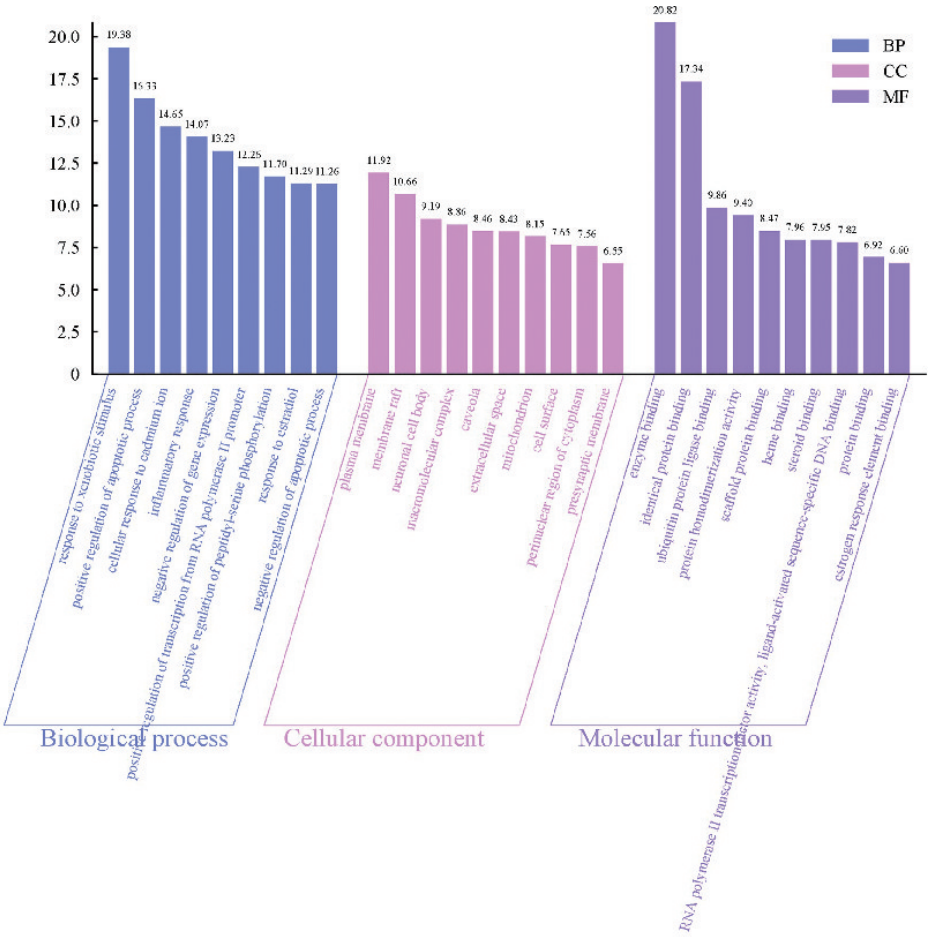

Fig. 3 GO pathway analysis of target genes

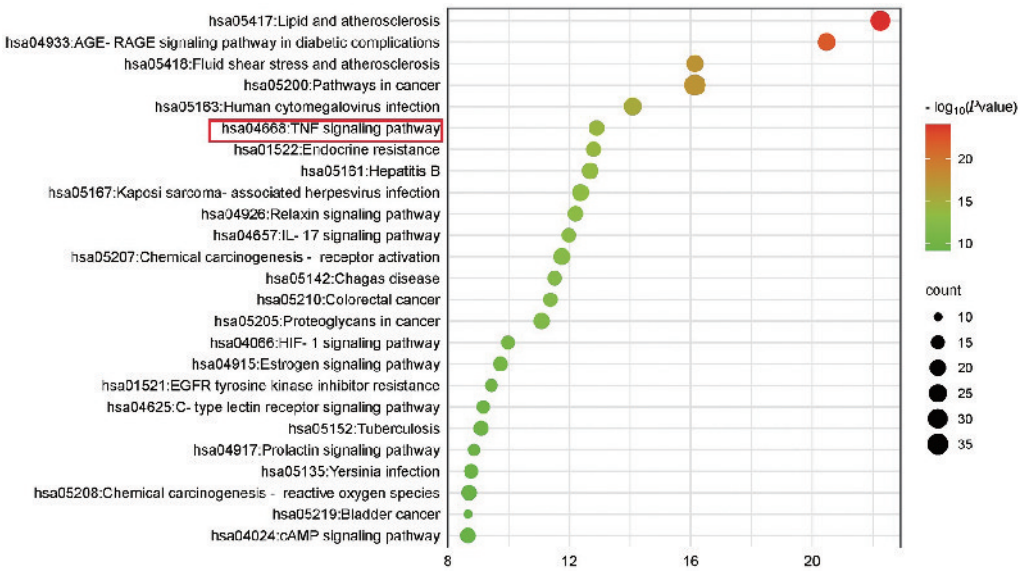

Fig. 4 KEGG pathway enrichment of target genes

3.2 Molecular docking

To assess whether the active ingredients in QHZYF act directly on TNF, we screened three active ingredients associated with TNF (Table 2) and conducted molecular docking analysis with TNFR1 and TNFR2 (Fig. 5). In the molecular docking process, the conformation of the small-molecule ligands was adjusted to binding to different protein receptors. The docking was repeated thrice for each group, the average binding energy was calculated (Fig. 6). Subsequently, we conducted *in vitro* and *in vivo* experiments to validate the efficacy and potential mechanisms of action of QHZYF in ameliorating post-MI depression.

Table 2　Molecular docking

Retention time	Ion mode	Components	Formula	mw	Calcd *m/z*	Obsed *m/z*	Error/ ($\times10^{-6}$)	MS/MS	Attribution
2.7	$[M+CH_3COO]^-$	Brazilein	$C_{16}H_{12}O_5$	284.068 5	343.081 8	343.080 7	3.21	229.053 0 $[M-H-C_3H_3O]^-$	Sappan Wood
4.02	$[M+H]^+$	Kaempferol	$C_{15}H_{10}O_6$	286.047 7	287.055 6	287.053 1	8.71	287.053 1$[M+H]^+$	Milkvetch Root and Safflower
5.55	$[M+H]^+$	Isorhamnetin	$C_{16}H_{12}O_7$	316.058 3	317.066 1	317.066 7	1.89	317.066 7$[M+H]^+$	Milkvetch Root

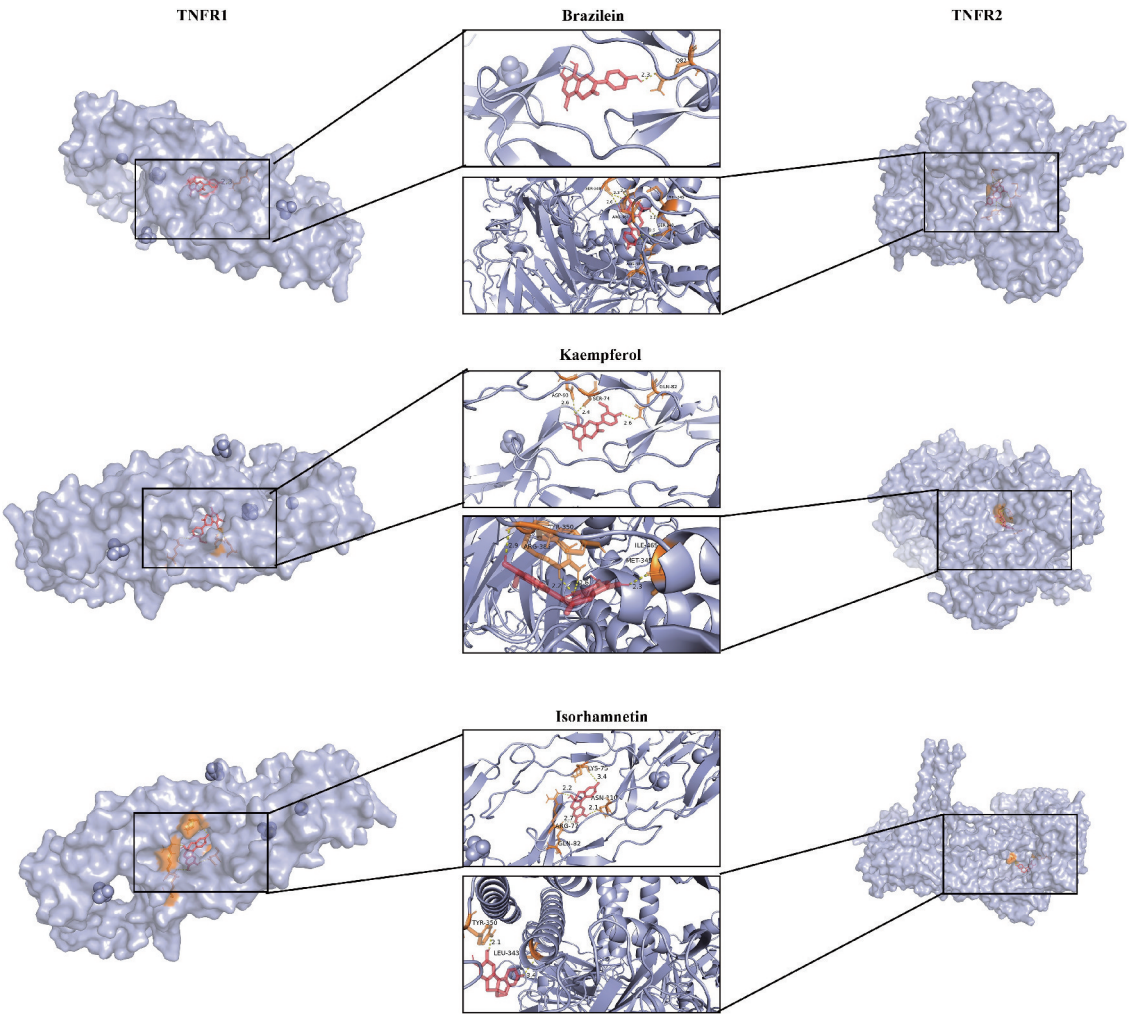

Fig. 5　3D visualisation of molecular docking of TNFR1, TNFR2 with brazilein, kaempferol, and isorhamnetin

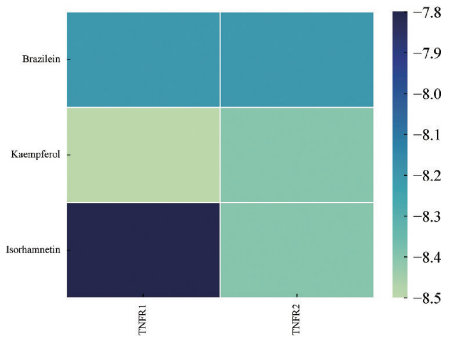

Fig. 6　Average binding energy heat map

3.3　QHZYF improves myocardial damage caused by MI

To evaluate the efficacy of QHZYF in treating post-MI depression, we constructed a rat model subjected to a 28-day restraint procedure three days after MI modelling, with QHZYF administered for 28 consecutive days (Fig. 7). Cardiac ultrasonography revealed significantly improved LVEF, LVFS, LVIDs, and LVIDd values in the treatment groups compared with the model group, with the most pronounced effect observed in the QHZYF-H group (Fig. 8). HE staining further revealed significant inflammatory cell infiltration in the heart tissue of the model group, while QHZYF significantly improved the inflammatory status of the infarct tissue (Fig. 9). Masson's trichrome staining showed extensive fibrin deposition in the heart tissue of the model group (Fig. 10). Meanwhile, QHZYF effectively reduced fibrin

deposition and improved myocardial fibrosis. The ultrastructure of the heart tissue was further observed by TEM. In the model group, the mitochondria exhibited abnormal morphology with disordered arrangement. However, QHZYF treatment significantly improved the mitochondrial structure and arrangement (Fig. 11). These results suggested that QHZYF repaired tissue damage after MI and alleviated inflammation and fibrosis.

3.4　QHZYF improves neuronal damage caused by depression after MI

Behavioural tests were performed on rats before modelling (week 0), after modelling (week 4), and after treatment (week 8). The model group exhibited significant depressive tendencies, while the sham operation group showed no significant differences compared to the control group in the open field test (Fig. 12), forced swimming test (Fig. 13) and sucrose preference test (Fig. 14). These results suggest that QHZYF significantly improved depressive behaviour in the model group, as demonstrated by forced swimming test, open field test, and sucrose preference test.

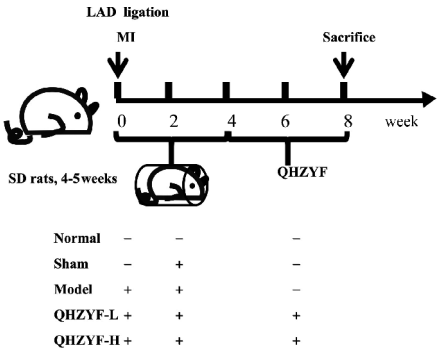

Fig. 7　Modelling of SD rats with post-MI depression

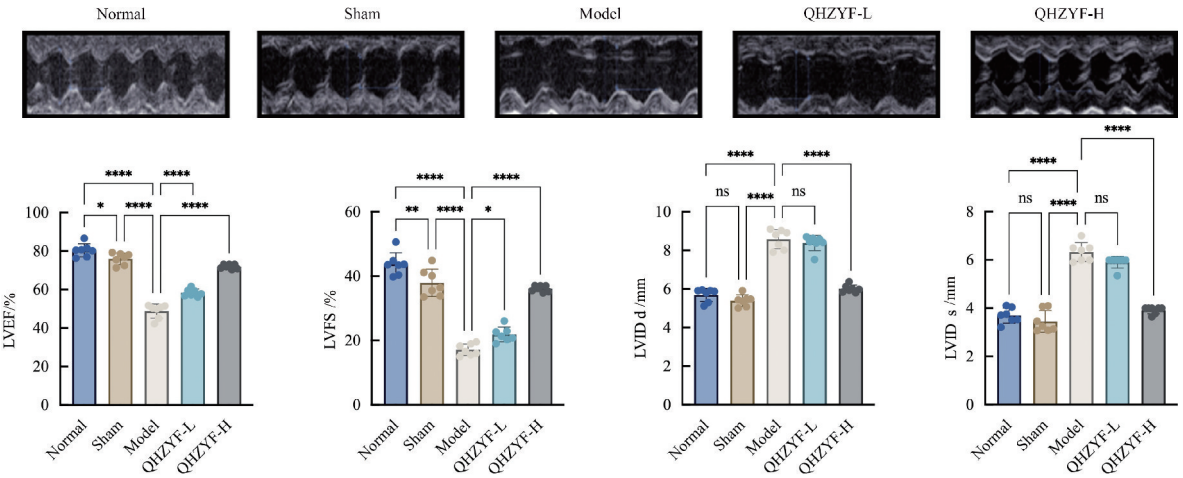

Note: The results are expressed as $\bar{x}\pm s$, $^{*}P<0.05$, $^{**}P<0.01$, $^{****}P<0.0001$, ns: not significant. $n=7$.

Fig. 8　Ultrasonic heart images and LVEF, LVFS, LVIDd, and LVIDs

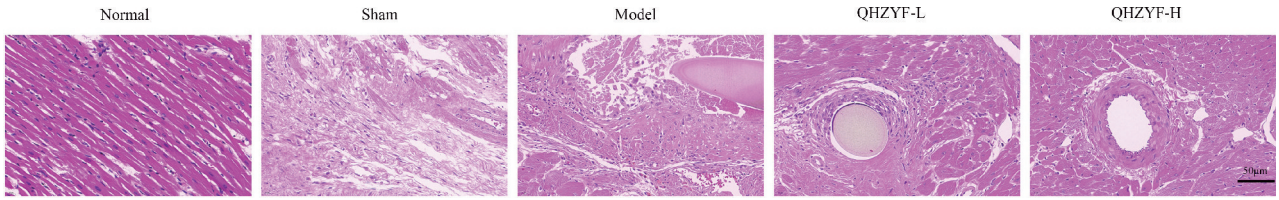

Fig. 9　HE staining of cardiac tissues (100×)

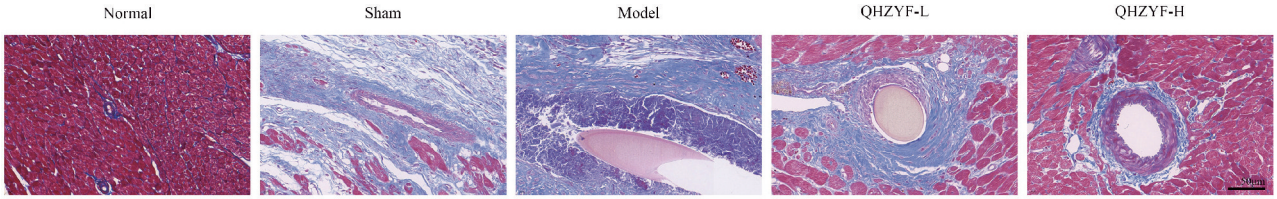

Fig. 10　Masson trichrome staining of cardiac tissues (100×)

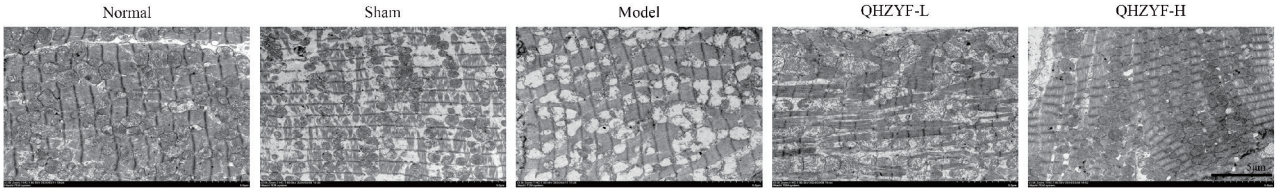

Fig. 11　TEM images of cardiac tissues (1 000×)

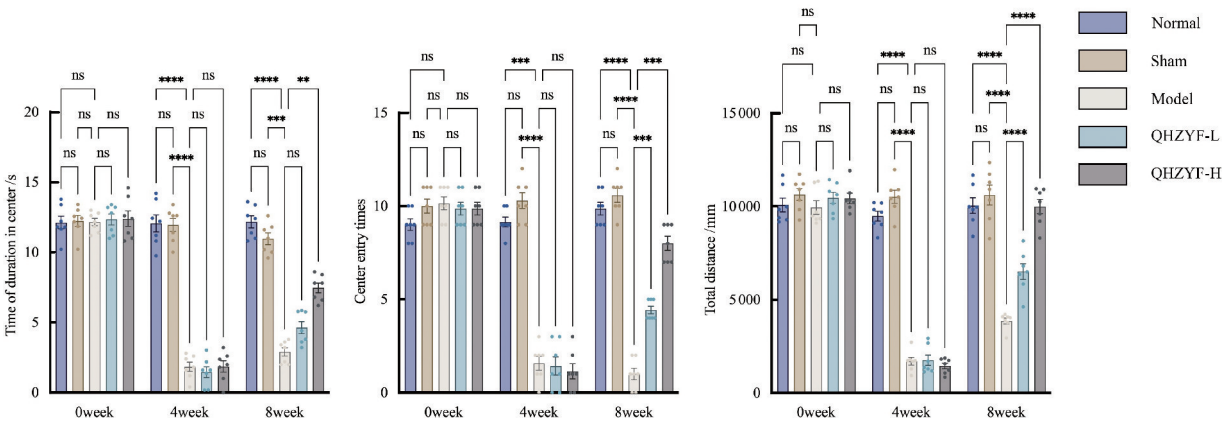

Note:The results are expressed as $\bar{x}\pm s$, $^{**}P<0.01$, $^{***}P<0.001$, $^{****}P<0.0001$, ns: not significant. $n=7$.

Fig. 12　Open field test

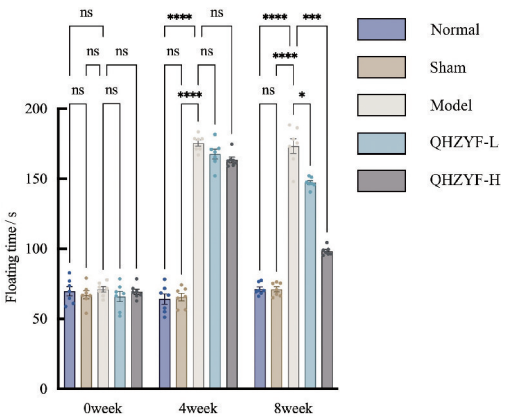

Note:The results are expressed as $\bar{x}\pm s$, $^{*}P<0.05$, $^{***}P<0.001$, $^{****}P<0.0001$, ns: not significant. $n=7$.

Fig. 13　Forced swimming test.

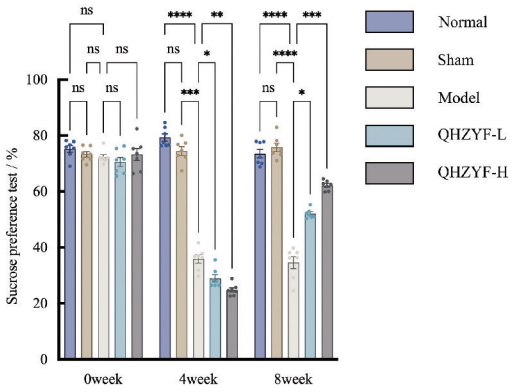

Note:The results are expressed as $\bar{x}\pm s$, $^{*}P<0.05$, $^{**}P<0.01$, $^{***}P<0.001$, $^{****}P<0.0001$, ns: not significant. $n=7$.

Fig. 14　Sucrose preference test

Nissl staining assessed morphological changes in the hippocampal tissue of depressed rats after MI. Nissl bodies in the model group exhibited morphological alterations characterized by chromatolysis, fragmentation into granular particles, perinuclear marginalization of residual material, and a significant reduction in cytoplasmic distribution area. Meanwhile, in the QHZYF-H group, neuronal damage were effectively reversed (Fig. 15).

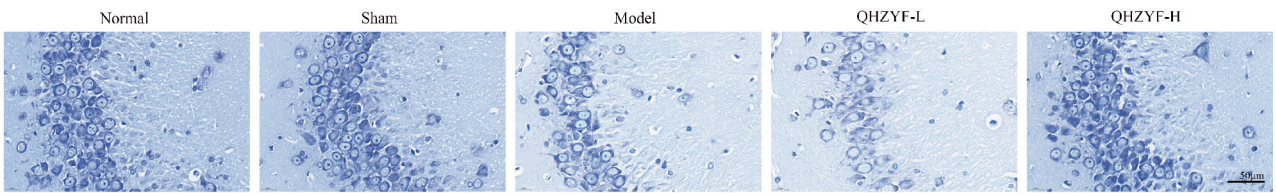

Fig. 15　Nissl staining of the rat hippocampus (100×)

3.5　QHZYF alleviates the inflammatory state of post-MI depression *in vivo* through the TNFR1/TNFR2 pathway

To investigate the potential mechanisms of action of QHZYF in treating post-MI depression, the abundance of proteins in the TNFR2/PI3K/AKT and TNFR1/NF-κB pathways were evaluated via Western blot within the heart (Fig. 16) and hippocampus (Fig. 17) of rats. TNFR2 expression in the heart and hippocampus of the model group was significantly decreased, where as TNFR1 was significantly increased. PI3K/AKT, the downstream pathway of TNFR2, showed decreased p-Akt levels in the model group, which was reversed by QHZYF treatment. The levels of p-NF-κB/NF-κB , a downstream target of TNFR1, were elevated in the model group and effectively inhibited by QHZYF. These results were confirmed via immunohistochemical staining in heart (Fig. 18) and hippocampus (Fig. 19).

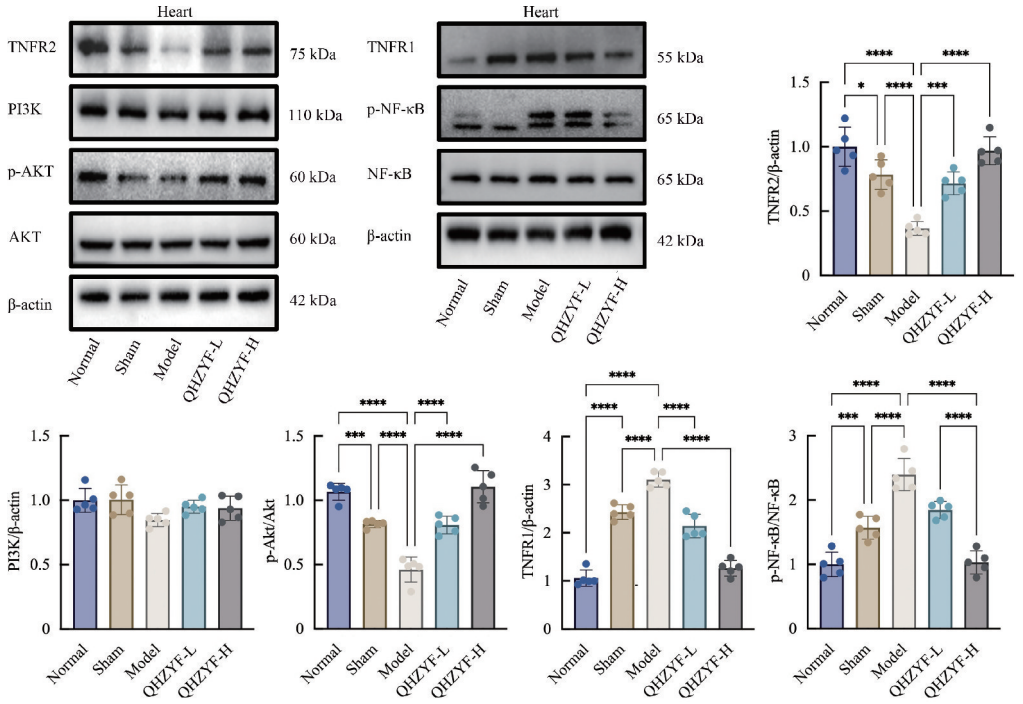

Note: The results are expressed as $\bar{x}\pm s$, $^{*}P<0.05$, $^{***}P<0.001$, $^{****}P<0.000\ 1$. $n=5$.

Fig. 16 Abundance of TNFR2, PI3K, p-AKT, AKT, TNFR1, NF-κB, p-NF-κB and β-actin proteins in heart of SD rats

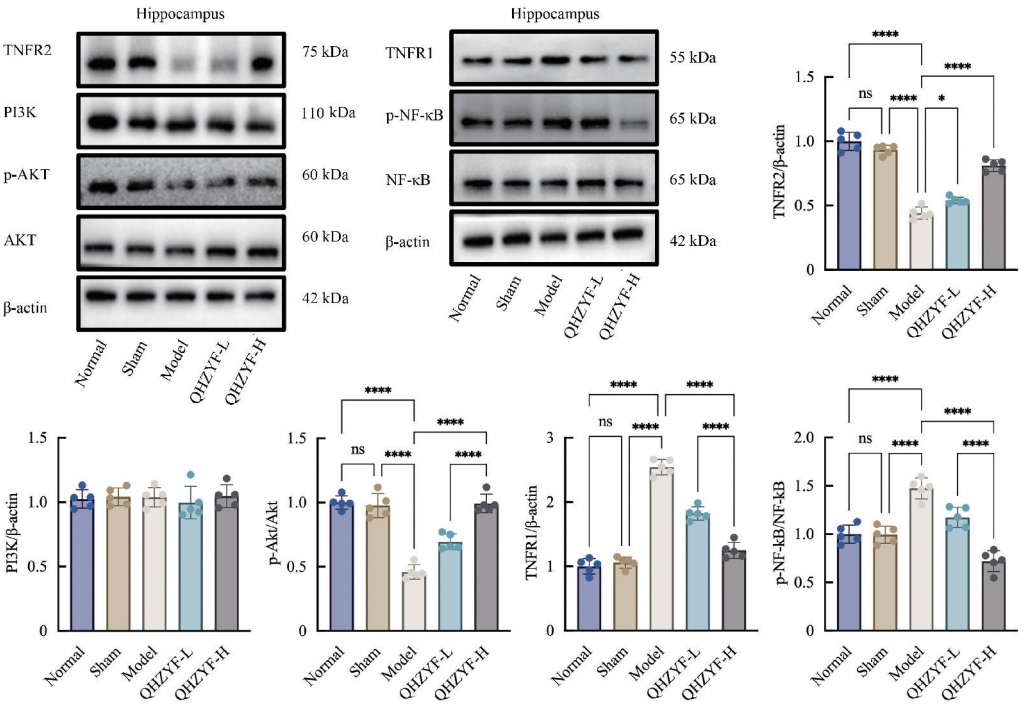

Note: The results are expressed as $\bar{x}\pm s$, $^{*}P<0.05$, $^{***}P<0.001$, $^{****}P<0.000\ 1$, ns: not significant. $n=5$.

Fig. 17 Abundance of TNFR2, PI3K, p-AKT, AKT, TNFR1, NF-κB, p-NF-κB, and β-actin proteins in hippocampus of SD rats

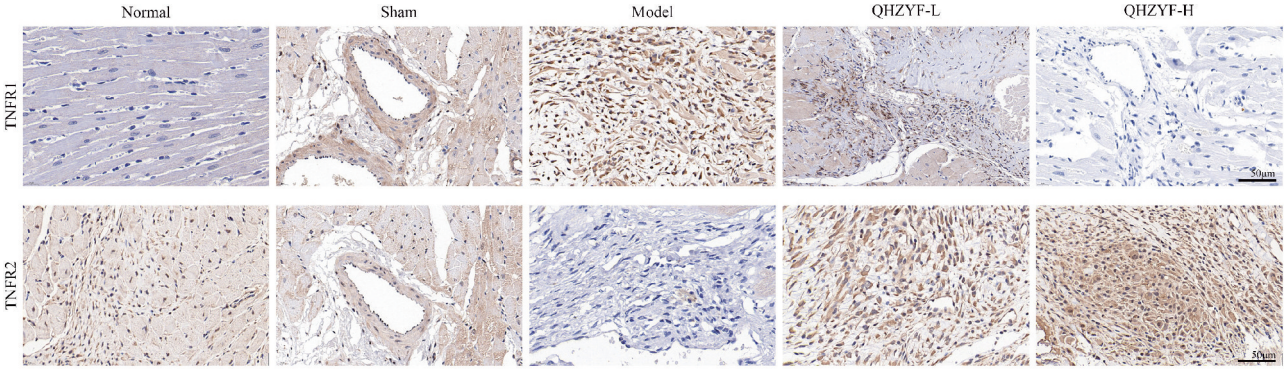

Fig. 18　Immunohistochemical staining of TNFR1 and TNFR2 in heart of post-MI SD rats (100×)

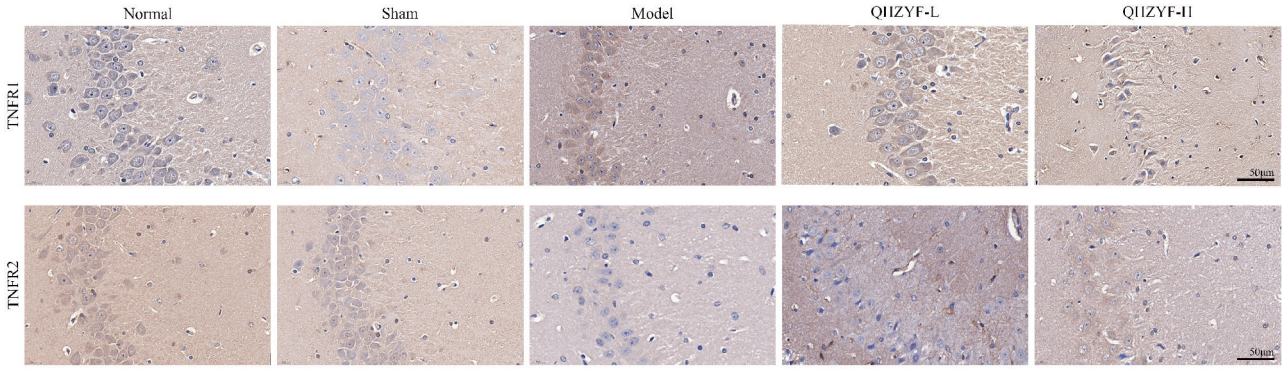

Fig. 19　Immunohistochemical staining of TNFR1 and TNFR2 in hippocampus of post-MI SD rats (100×)

Additionally, serum levels of the pro-inflammatory factor IL-6 and the anti-inflammatory factor IL-10 were significantly increased in the model group, while QHZYF effectively reduced IL-6 and increased IL-10 levels(Fig. 20). Collectively, these results suggest that QHZYF may improve post-MI depression by modulating the TNFR2/PI3K/AKT and TNFR1/NF-κB pathways while restoring the balance between pro-inflammatory and anti-inflammatory factors.

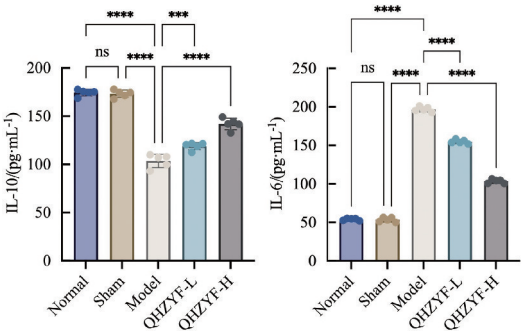

Note: The results are expressed as $\bar{x}\pm s$, $^{***}P<0.001$, $^{****}P<0.0001$, ns: not significant. $n=5$.

Fig. 20　Serum IL-6 and IL-10 levels.

3.6　QHZYF improves cellular inflammation *in vitro* through the TNFR1/TNFR2 pathway

To explore the potential mechanism by which QHZYF ameliorated myocardial cell and neuronal damage after MI, we constructed an *in vitro* model of post-MI depression (Fig. 21). We determined the optimal time point for cell co-culture through CCK-8 (Fig. 22A). To explore the mechanism by which QHZYF regulates TNFR1/TNFR2, a CCK-8 assay determined that the optimal concentration of QHZYF for intervention in H9C2 and PC12 cells was 12% (Fig. 22B).

Western blot analysis revealed that in H9C2 (Fig. 23) and PC12 cells (Fig. 24), the levels of TNFR2 and p-AKT/AKT were higher in the QHZYF-treated group than in the C-6His (TNFR2 agonist) or H398 (TNFR1 inhibitor) groups ($P<0.01$). In contrast, the levels of TNFR1 and p-NF-κB / NF-κB expression were lower in the QHZYF-treated group than in the C-6His and H398 groups ($P<0.01$). Notably, compared with the H398 group, QHZYF+H398 significantly increased TNFR2 and p-AKT / AKT expression in H9C2 and PC12 cells($P<0.01$), additionally, TNFR1 and p-NF-κB/ NF-κB levels were inhibited in cells ($P<0.01$). Compared with the C-6His group, QHZYF+C-6His treatment increased TNFR2 and p-AKT/AKT while decreasing that of TNFR1 and p-NF-κB/ NF-κB in H9C2 and PC12 cells ($P<0.01$).

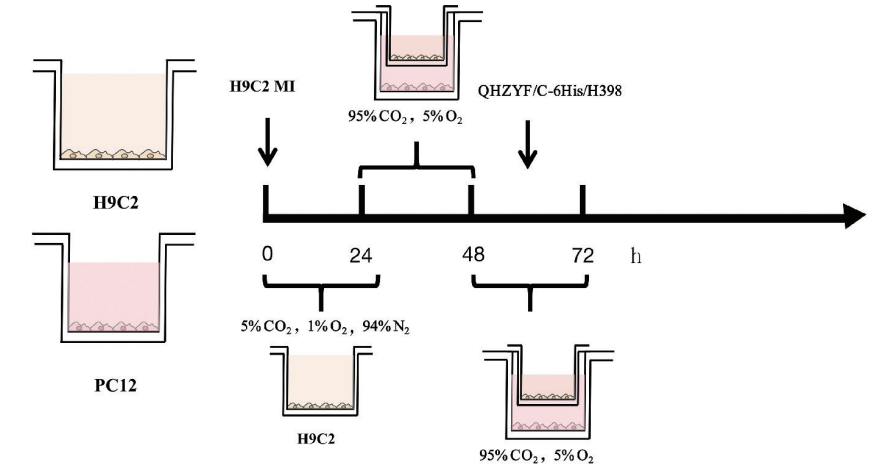

Fig. 21　cell culture model construction and administration

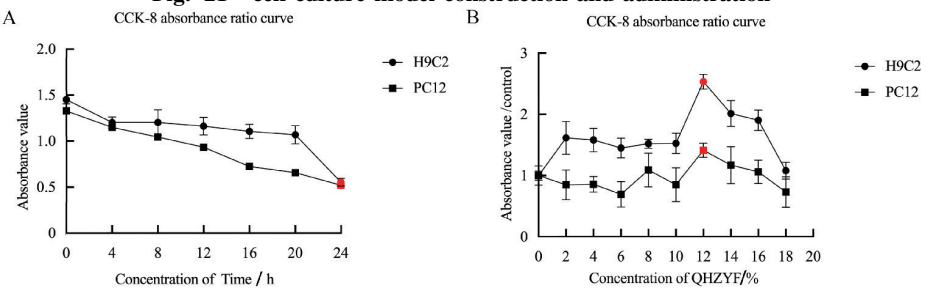

Note：（A）CCK-8 analysis following hypoxia treatment of H9C2 cells and co-culture with PC12 cells；（B）Optimal concentration of QHZYF-containing serum for treating H9C2 and PC12 cells.

Fig. 22　Cell viability was detected by the CCK-8 assay

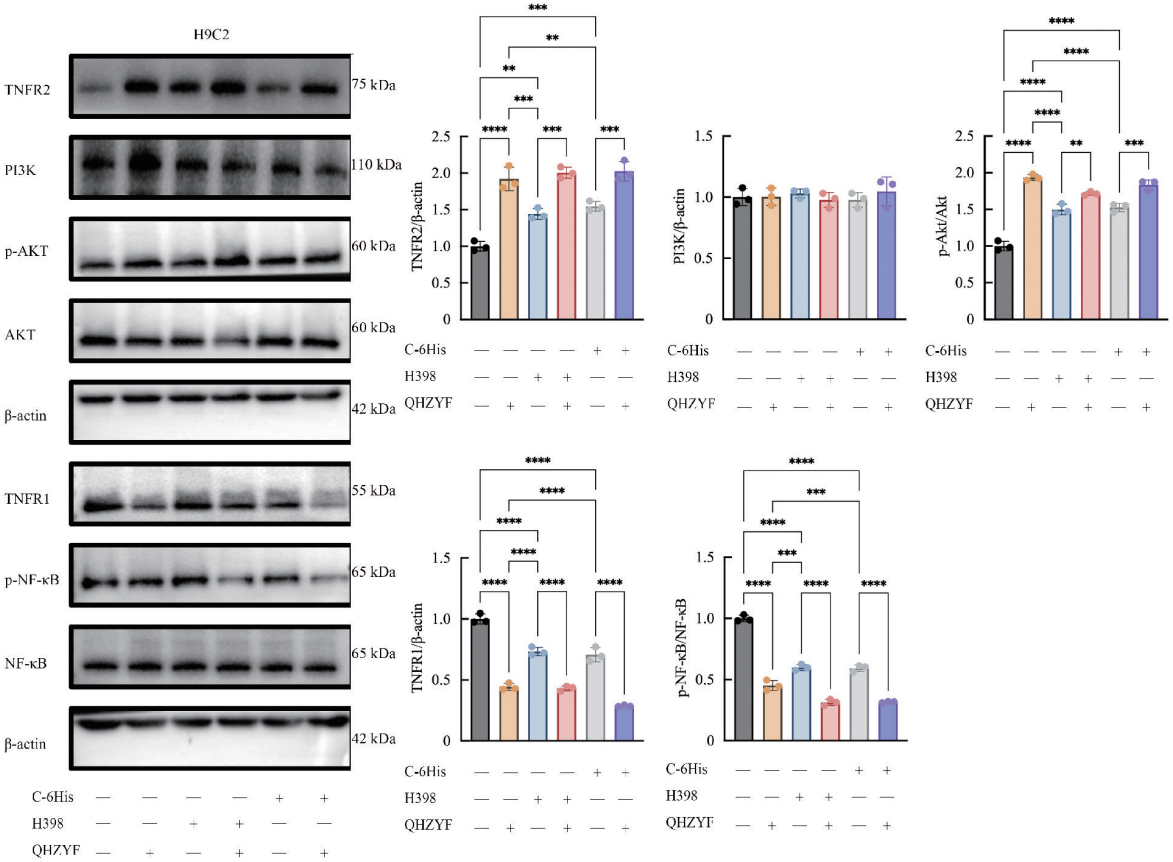

Note：The results are expressed as $\bar{x}\pm s$，$^{**}P<0.01$，$^{***}P<0.001$，$^{****}P<0.0001$. $n=3$.

Fig. 23　Abundance of TNFR2，PI3K，p-AKT，AKT，TNFR1，p-NF-κB，NF-κB and β-actin in H9C2 cells

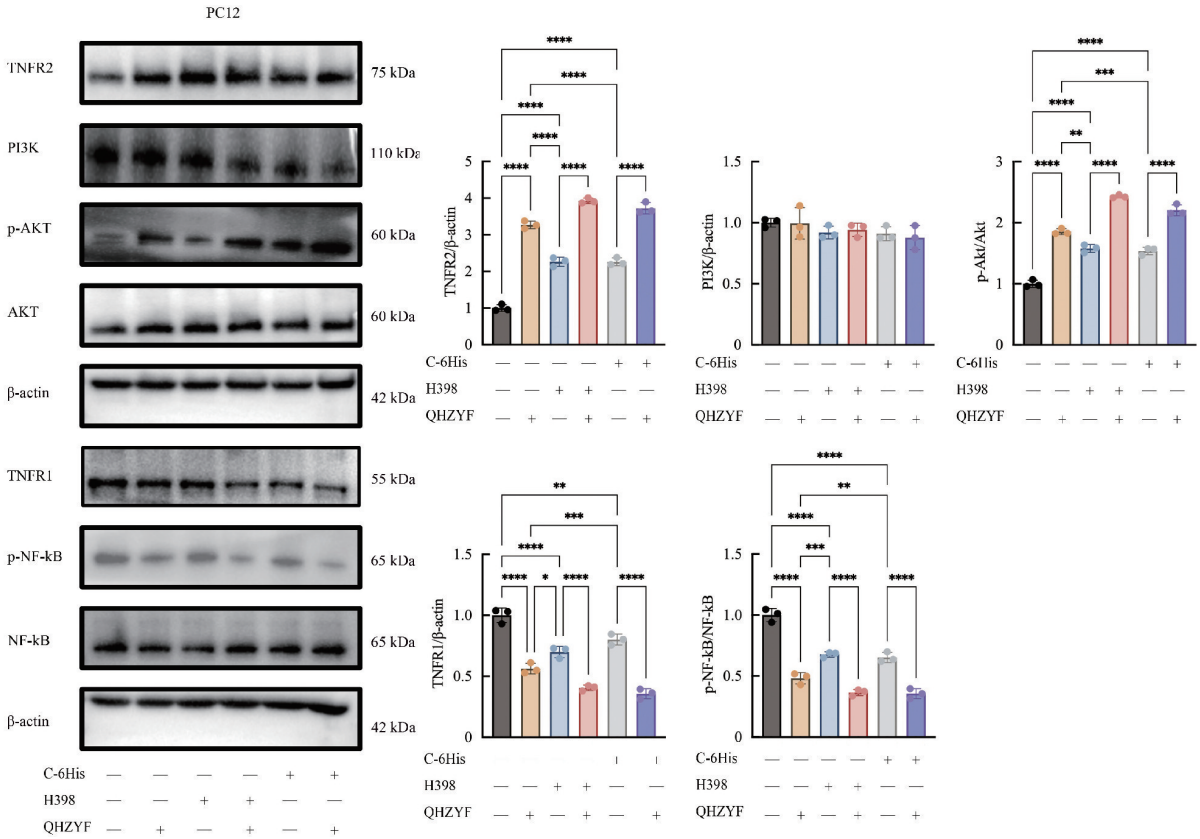

Note:The results are expressed as $\bar{x}\pm s$, $^{*}P<0.05$, $^{**}P<0.01$, $^{***}P<0.001$, $^{****}P<0.000\ 1$. $n=3$.

Fig. 24　Abundance of TNFR2, PI3K, p-AKT, AKT, TNFR1, p-NF-κB, NF-κB and β-actin in PC12 cells

TUNEL staining revealed that QHZYF+C-6His and QHZYF +H398 significantly decreased apoptosis and promoted cell viability, outperforming monotreatment with C - 6His or H398 (Fig. 25) ($P<0.01$). In addition, in the H9C2 cellular supernatant, QHZYF promoted IL-10 expression and inhibited IL-6 expression. Combinatorial treatment (QHZYF + C - 6His or QHZYF+H398) enhanced this effect. A similar trend was observed in the PC12 cells (Fig. 26) ($P<0.01$).

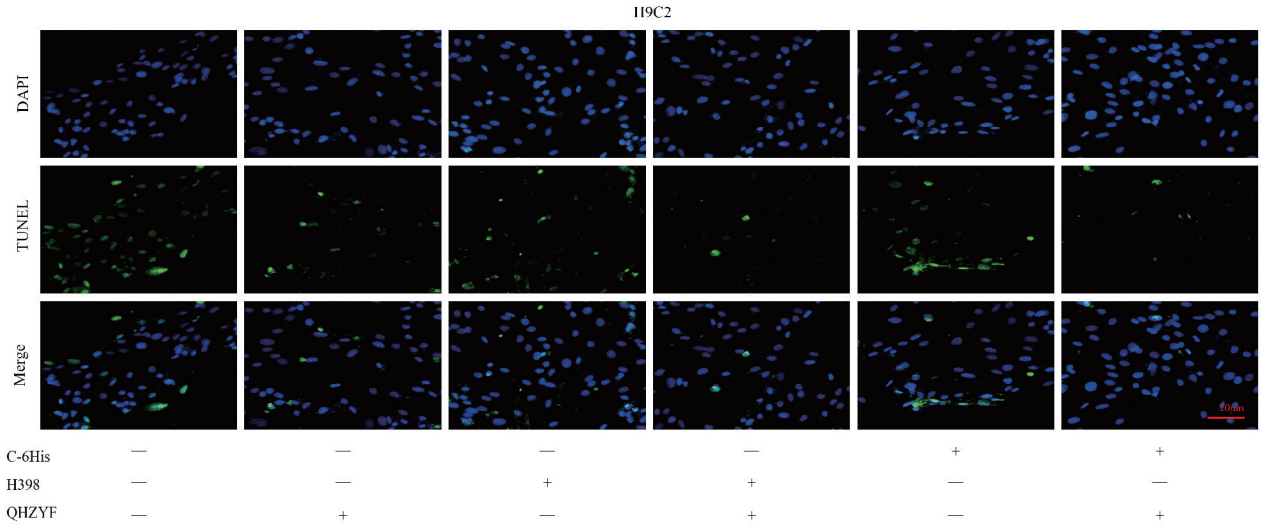

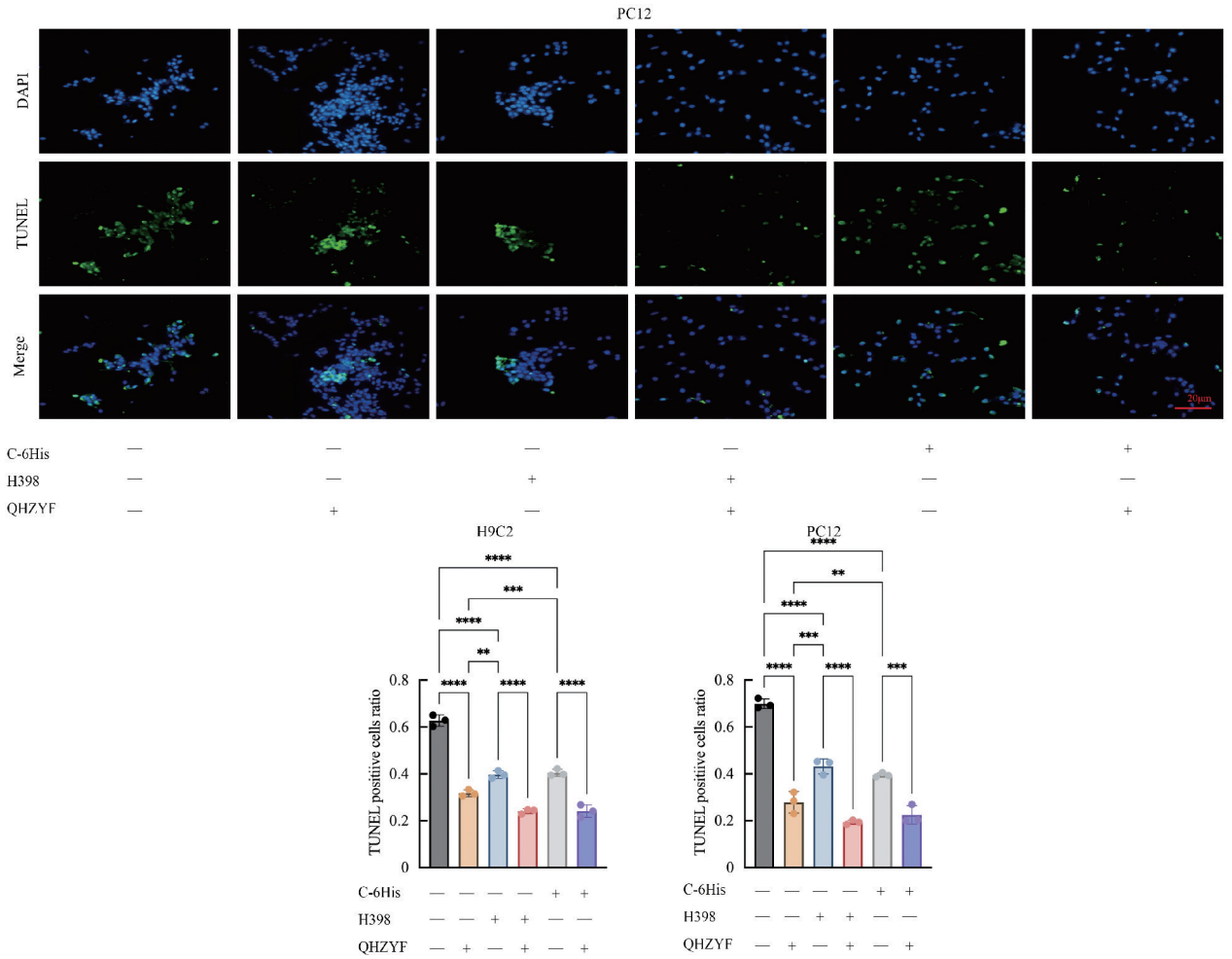

Note: The results are expressed as $\bar{x}\pm s$, $^{**}P<0.01$, $^{***}P<0.001$, $^{****}P<0.0001$. $n=3$, 200×.

Fig. 25　Apoptosis of H9C2 and PC12 cells detected by TUNEL staining

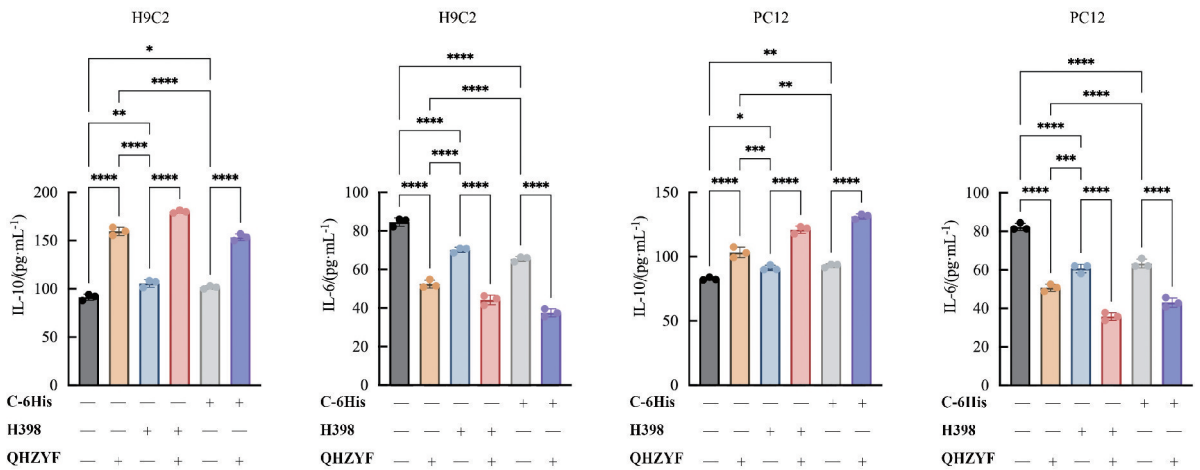

Note: The results are expressed as $\bar{x}\pm s$, $^{*}P<0.05$, $^{**}P<0.01$, $^{***}P<0.001$, $^{****}P<0.0001$. $n=3$.

Fig. 26　Expression of IL-6 and IL-10 in the supernatant of H9C2 and PC12 cell cultures.

4　Discussion

Although the pathological mechanism of post-MI depression is complex, QHZYF exerts promising therapeutic efficacy for clinical applications. This study explores the mechanisms by which QHZYF treats post-MI depression using network pharmacology, focusing specifically on the regulation of TNF and its signalling pathways.

Brazilein, kaempferol, and isorhamnetin were identified as the main active components of QHZYF that alleviated the symptoms of post-MI depression. These components exhibited a high affinity for two TNF receptors (TNFR1 and TNFR2). After MI, the TNF levels in the heart, peripheral blood, and central nervous system are significantly elevated[24], worsening cardiovascular prognosis and negative emotional states[25]. Indeed, TNF-α

is closely associated with MI, atherosclerosis, chronic heart failure, and other cardiac injuries[26]. Hence, TNF may trigger brain-heart inflammation post-MI depression. However, TNF inhibition alone did not yield the expected therapeutic effect, highlighting the complexity of TNF-related signalling pathways[27-28]. Following acute MI, TNF-α mediates inflammatory responses through TNFR1 and TNFR2 receptors[29]. However, the specific synergistic mechanisms underlying these processes remain unclear.

We hypothesised that QHZYF restores inflammatory homeostasis by modulating TNFR1 and TNFR2. To test this hypothesis, we successfully established a rat model of post-MI depression by ligating the left anterior descending coronary artery and restricting movement post-surgery to simulate the long-term bed rest required after an MI. As the core region of the limbic system, the hippocampus is critical in emotion regulation, while its dysfunction is closely related to depression[30]. Therefore, we selected the hippocampus as the main target for studying depressive states *in vivo*. However, considering that the hippocampus is also involved in pain regulation[31], a sham operation group was included to avoid interference from pain in evaluating behavioural depression in an MI model. Our experiments revealed significant differences in both cardiac and neurological function between the model and sham groups. While cardiac function also differed significantly between the sham and normal groups, no such differences were observed in neurological function or depressive-like behaviors. Critically, these findings establish that MI itself rather than the surgical trauma constitutes the primary pathological basis for the subsequent development of depression-like behaviors. Consequently, the depressive-like behaviors and hippocampal alterations observed in the model group animals predominantly stem from the pathophysiological processes triggered by MI, not non-specific effects of the sham surgical procedure. Compared with the model group, QHZYF intervention significantly improved cardiac function and emotional state, playing a key role in enhancing both cardiac function and behavioural outcomes in post-MI depression.

TNF-α is often considered a major driver of pro-inflammatory responses and tissue damage in pathological processes; however, its role in the heart is more complex[32]. TNF-α antagonists provide short-term benefits for patients in the compensatory stage of heart failure, but their long-term use may worsen this condition[28,33]. TNFR1 activation is associated with adverse remodelling and heart dysfunction after MI, while TNFR2 activation has anti-inflammatory and protective effects[34-36]. For example, in a TNFR1 knockout model, systolic heart function improved significantly after MI, accompanied by reduced expression of inflammatory markers, suggesting that TNFR1 signalling contributes to the inflammatory response[37]. In contrast, TNFR2 knockdown worsens ventricular dilation, impairs cardiac function, and intensifies the inflammatory response, demonstrating its anti-inflammatory and protective effects. Therefore, studying the regulatory balance between TNFR1 and TNFR2 under different pathological conditions is crucial for optimising TNF-α-based treatment strategies.

Although TNFR1 and TNFR2 share certain factors associated with TNF signalling, they coordinate inflammatory responses or maintain homeostasis by activating distinct downstream signalling pathways[38]. Moreover, while the extracellular ligand-binding domains of TNFR1 and TNFR2 share significant structural homology, they differ in their intracellular signalling structures, which form a key basis for the multidirectionality of TNF signalling. The intracellular region of TNFR1 contains a death domain (DD), enabling the recruitment of adaptor proteins such as TRADD and receptor-interacting serine/threonine kinase 1 (RIPK1). Subsequently, TNF receptor-associated factor-2 (TRAF2) and apoptosis inhibitors (cIAP1 and cIAP2) are recruited. These molecules activate NF-κB expression and its downstream genes, potentially inducing apoptosis, necrosis, and reactive oxygen species (ROS) production[39]. In contrast, TNFR2 lacks a DD and thus cannot directly mediate apoptotic signalling. Rather, TNFR2 activates the classical NF-κB pathway by recruiting TRAF2, which has multiple immunomodulatory functions[40-41]. TNFR2 can also activate the PI3K/AKT signalling pathway by interacting with the cytoplasmic tyrosine kinase BMX, which is closely related to tissue repair and anti-inflammatory effects[42]. Notably, TNFR2 can also independently interact with other signalling proteins.

TNF-α negatively regulates hippocampal neurogenesis[43]. Although the present study could not clearly distinguish between the central and peripheral sources of the effect of TNF, the intricate communication between the central and peripheral immune systems cannot be ignored. This is primarily mediated by TNF and other cytokines and can occur without direct damage to the BBB[44]. TNF can cross the BBB and enter the central nervous system through TNFR1 and TNFR2 dependent mechanisms[45-48]. This process may represent a key pathway through which peripheral injury induces central nervous inflammation and affects hippocampal neuroplasticity.

We also found that in the brains of mice after MI, TNF precursor protein levels significantly increased, accompanied by a near doubling of TNFR1 expression, while TNFR2 expression significantly decreased. This suggests that neuroinflammation may persist after MI, having long-term effects on brain-heart interactions[49]. Microglia, the immune cells of the brain, are activated when stimulated, whereas astrocytes participate in the brain-heart inflammatory network after MI[50]. TNFR2 agonists improved microglial activity and cardiac function while exerting limited effects on overall inflammation and behavioural improvements. Although TNFR1 antagonists do not improve cardiac function, they increase neuroinflammation and sympathetic nerve activity[27]. Hence, treatment strategies targeting TNFR1 inhibition or TNFR2 activation alone may be insufficient to effectively improve neuroinflammation and cardiac function after MI. Thus, developing a therapeutic regimen that balances TNFR1 and TNFR2 activity may be key to coordinating inflammation regulation between the heart and the brain, improving post-MI neuroinflammation, cardiac function, and related behavioural abnormalities.

Mechanistically, QHZYF balanced TNFR1/TNFR2 activity, inhibited over-activation of the TNFR1/NF-κB signalling pathway, reduced inflammation and damage, and activated the TNFR2/PI3K/AKT signalling pathway. This significantly reduces serum pro-inflammatory factor IL-6 levels while up-regulating the anti-inflammatory factor IL-10, playing a dual role in immune regulation and anti-inflammatory repair.

Signal crosstalk between TNFR1 and TNFR2 may be a key mechanism underlying their synergistic effect in regulating inflammation. TNFR2 may indirectly affect TNFR1-mediated apoptotic signalling by regulating the availability of TRAF2. Simultaneously, TNFR1-mediated inflammatory signalling may regulate tissue repair and immune homeostasis by altering TNFR2 activity[39,51-52]. The interaction between TNFR1 and TNFR2 may be related to the two active forms of TNF-α. TNF-α can exist in a membrane-bound (tm-TNF-α) or soluble (sTNF-α) form, with sTNF-α being converted by TNF-α converting

enzyme[53]. tm-TNF-α activates TNFR1 and TNFR2, whereas sTNF-α only activates TNFR1[54]. Nevertheless, both receptors mediate apoptotic signals; however, their regulation differs significantly[55-56]. To verify the crosstalk between TNFR1 and TNFR2, *in vitro* experiments were conducted in the current study in which H9C2 cells exposed to hypoxia were co-cultured with PC12 cells to construct myocardial and neuronal injury models. To further investigate QHZYF's contribution to TNFR1/TNFR2 synergistic signaling, we evaluated sera containing varying concentrations of QHZYF. This screening identified 12% QHZYF as the optimal concentration for subsequent interventions. Furthermore, in H9C2 and PC12 cell models, QHZYF exhibited stronger anti-apoptotic and anti-inflammatory effects than TNFR1 antagonists or TNFR2 agonists alone. However, when QHZYF was combined with a TNFR1 antagonist or TNFR2 agonist, its efficacy was significantly amplified compared with those elicited by any single agent. These results demonstrate the synergistic regulation of TNFR1 and TNFR2, highlighting QHZYF's anti-inflammatory and cell protective effects. This suggests that maintaining a balance between TNFR1 and TNFR2 may have greater therapeutic potential for inflammation and immune regulation than a single TNFR1 suppression or TNFR2 activation strategy.

This study has certain limitations. First, the pathological mechanisms of depression after MI may extend beyond the hippocampal region and involve the regulation of the hypothalamic-pituitary-adrenal axis, BBB permeability, and functional changes in the prefrontal cortex. It may also include abnormal lipid metabolism and pathological changes in related cells that were not investigated in this study. Second, we did not evaluate whether TNFR1/TNFR2-mediated immune homeostasis is influenced by the duration or concentration dynamics of inflammatory responses, warranting further investigation to better understand the complex pathological mechanisms after MI depression. Finally, while p-AKT(Ser473) is a primary indicator of PI3K/AKT pathway activation[57-58], future studies should directly evaluate upstream p-PI3K dynamics to fully elucidate the signaling cascade.

5 Conclusion

QHZYF effectively alleviates MI-induced myocardial injury and depression by improving the brain-heart inflammation imbalance. *In vivo*, QHZYF significantly improves the inflammatory state and degree of fibrosis in myocardial tissue, as well as hippocampal neuroplasticity. Mechanistically, QHZYF modulates inflammation in the heart and hippocampus through the TNFR1/NF-κB and TNFR2/PI3K/AKT signalling pathways. The efficacy of QHZYF is primarily attributed to its key active ingredients, including brazilein, kaempferol, and isorhamnetin. Thus, QHZYF improves myocardial injury and depressive symptoms by regulating brain-heart inflammatory homeostasis, representing a promising therapeutic strategy for post-MI depression.

References:

[1] KAUFMANN M W, FITZGIBBONS J P, SUSSMAN E J, et al. Relation between myocardial infarction, depression, hostility, and death[J]. Am Heart J, 1999, 138(3 Pt 1): 549-554.

[2] LADWIG K H, KIESER M, KONIG J, et al. Affective disorders and survival after acute myocardial infarction. Results from the post-infarction late potential study[J]. Eur Heart J, 1991, 12(9): 959-964.

[3] SMOLDEREN K G, BUCHANAN D M, GOSCH K, et al. Depression treatment and 1-year mortality after acute myocardial infarction: Insights from the TRIUMPH registry (translational research investigating underlying disparities in acute myocardial infarction patients' health status)[J]. Circulation, 2017, 135(18): 1681-1689.

[4] DE JONGE P, VAN DEN BRINK R H S, SPIJKERMAN T A, et al. Only incident depressive episodes after myocardial infarction are associated with new cardiovascular events[J]. J Am Coll Cardiol, 2006, 48(11): 2204-2208.

[5] THOMBS B D, DE JONGE P, COYNE J C, et al. Depression screening and patient outcomes in cardiovascular care: A systematic review[J]. JAMA, 2008, 300(18): 2161-2171.

[6] THACKERAY J T, HUPE H C, WANG Y, et al. Myocardial inflammation predicts remodeling and neuroinflammation after myocardial infarction[J]. J Am Coll Cardiol, 2018, 71(3): 263-275.

[7] GE Y B, XU W, ZHANG L J, et al. Ginkgolide B attenuates myocardial infarction-induced depression-like behaviors via repressing IL-1β in central nervous system[J]. Int Immunopharmacol, 2020, 85: 106652.

[8] WANG H W, AHMAD M, JADAYEL R, et al. Inhibition of inflammation by minocycline improves heart failure and depression-like behaviour in rats after myocardial infarction[J]. PLoS One, 2019, 14(6): e0217437.

[9] ADZIC M, BRKIC Z, MITIC M, et al. Therapeutic strategies for treatment of inflammation-related depression[J]. Curr Neuropharmacol, 2018, 16(2): 176-209.

[10] CHENG Y Y, DESSE S, MARTINEZ A, et al. TNFα disrupts blood brain barrier integrity to maintain prolonged depressive-like behavior in mice[J]. Brain Behav Immun, 2018, 69: 556-567.

[11] JOHANSSON P, LESMAN-LEEGTE I, SVENSSON E, et al. Depressive symptoms and inflammation in patients hospitalized for heart failure[J]. Am Heart J, 2011, 161(6): 1053-1059.

[12] PASIC J, LEVY W C, SULLIVAN M D. Cytokines in depression and heart failure[J]. Psychosom Med, 2003, 65(2): 181-193.

[13] IASELLA C J, KREIDER M S, HUANG L, et al. Effect of selective serotonin reuptake inhibitors on cardiovascular outcomes after percutaneous coronary intervention: A retrospective cohort study[J]. Clin Drug Investig, 2019, 39(6): 543-551.

[14] COLPO G D, LEBOYER M, DANTZER R, et al. Immune-based strategies for mood disorders: Facts and challenges[J]. Expert Rev Neurother, 2018, 18(2): 139-152.

[15] GROSSER T, RICCIOTTI E, FITZGERALD G A. The cardiovascular pharmacology of nonsteroidal anti-inflammatory drugs[J]. Trends Pharmacol Sci, 2017, 38(8): 733-748.

[16] HUANG L L, XU R, HUANG X, et al. Traditional Chinese medicine injection for promoting blood circulation and removing blood stasis in treating angina pectoris of coronary heart disease: A protocol for systematic review and network meta-analysis[J]. Medicine, 2021, 100(16): e25608.

[17] ZHANG Y T, QIN S, WANG X Q, et al. The scientific connotation of "heart and brain co-dominating the mind" and its application in the treatment of insomnia by acupuncture[J]. J Nanjing Univ Tradit Chin Med, 2025, 41(2): 181-188.

[18] NI W B, YAO Z P, GE F Q, et al. Clinical research of Shuangxin decoction on coronary heart disease accompanied with psychological disorder[J]. J Nanjing Univ Tradit Chin Med, 2017, 33(1): 26-29.

[19] DU W D. TCM therapeutic principles for treatment of psychosomatic diseases[J]. J Nanjing Univ Tradit Chin Med, 2000, 16(6): 335-337.

[20] CHENG S Y, ZHANG X X, FENG Q, et al. Astragaloside IV exerts angiogenesis and cardioprotection after myocardial infarction via regulating PTEN/PI3K/Akt signaling pathway[J]. Life Sci, 2019, 227: 82-93.

[21] DING Y H, XIANG Q, ZHU P Y, et al. Qihuang Zhuyu formula alleviates coronary microthrombosis by inhibiting PI3K/Akt/αIIbβ3-mediated platelet activation[J]. Phytomedicine, 2024, 125: 155276.

[22] NAIR A, MORSY M A, JACOB S. Dose translation between laboratory animals and human in preclinical and clinical phases of drug development[J]. Drug Dev Res, 2018, 79(8): 373-382.

[23] PIAO L M, ZHAO G X, ZHU E B, et al. Chronic psychological stress accelerates vascular senescence and impairs ischemia-in-

duced neovascularization: The role of dipeptidyl peptidase-4/glucagon-like peptide-1-adiponectin axis[J]. J Am Heart Assoc, 2017, 6(10): e006421.
[24] REN W J, LIU Y, ZHOU L J, et al. Peripheral nerve injury leads to working memory deficits and dysfunction of the hippocampus by upregulation of TNF-α in rodents[J]. Neuropsychopharmacology, 2011, 36(5): 979-992.
[25] LIU H, LUITEN P G M, EISEL U L M, et al. Depression after myocardial infarction: TNF-α-induced alterations of the blood-brain barrier and its putative therapeutic implications[J]. Neurosci Biobehav Rev, 2013, 37(4): 561-572.
[26] KLEINBONGARD P, HEUSCH G, SCHULZ R. TNFalpha in atherosclerosis, myocardial ischemia/reperfusion and heart failure[J]. Pharmacol Ther, 2010, 127(3): 295-314.
[27] GOUWELEEUW L, WAJANT H, MAIER O, et al. Effects of selective TNFR1 inhibition or TNFR2 stimulation, compared to non-selective TNF inhibition, on (neuro) inflammation and behavior after myocardial infarction in male mice[J]. Brain Behav Immun, 2021, 93: 156-171.
[28] BOZKURT B, TORRE-AMIONE G, WARREN M S, et al. Results of targeted anti-tumor necrosis factor therapy with etanercept (ENBREL) in patients with advanced heart failure[J]. Circulation, 2001, 103(8): 1044-1047.
[29] SCHULZ R, HEUSCH G. Tumor necrosis factor-alpha and its receptors 1 and 2: Yin and Yang in myocardial infarction? [J]. Circulation, 2009, 119(10): 1355-1357.
[30] CASTREN E. Is mood chemistry? [J]. Nat Rev Neurosci, 2005, 6(3), 241-246.
[31] MUTSO A A, RADZICKI D, BALIKI M N, et al. Abnormalities in hippocampal functioning with persistent pain[J]. J Neurosci, 2012, 32(17): 5747-5756.
[32] LIU H, LUITEN P G M, EISEL U L M, et al. Depression after myocardial infarction: TNF-α-induced alterations of the blood-brain barrier and its putative therapeutic implications[J]. Neurosci Biobehav Rev, 2013, 37(4): 561-572.
[33] CHUNG E S, PACKER M, LO K H, et al. Randomized, double-blind, placebo-controlled, pilot trial of infliximab, a chimeric monoclonal antibody to tumor necrosis factor-alpha, in patients with moderate-to-severe heart failure: Results of the anti-TNF Therapy Against Congestive Heart Failure (ATTACH) trial[J]. Circulation, 2003, 107(25): 3133-3140.
[34] DUERRSCHMID C, CRAWFORD J R, REINEKE E, et al. TNF receptor 1 signaling is critically involved in mediating angiotensin-II-induced cardiac fibrosis[J]. J Mol Cell Cardiol, 2013, 57: 59-67.
[35] HIGUCHI Y, MCTIERNAN C F, FRYE C B, et al. Tumor necrosis factor receptors 1 and 2 differentially regulate survival, cardiac dysfunction, and remodeling in transgenic mice with tumor necrosis factor-alpha-induced cardiomyopathy[J]. Circulation, 2004, 109(15): 1892-1897.
[36] GARLIE J B, HAMID T, GU Y, et al. Tumor necrosis factor receptor 2 signaling limits β-adrenergic receptor-mediated cardiac hypertrophy *in vivo*[J]. Basic Res Cardiol, 2011, 106(6): 1193-1205.
[37] RAMANI R, MATHIER M, WANG P, et al. Inhibition of tumor necrosis factor receptor-1-mediated pathways has beneficial effects in a murine model of postischemic remodeling[J]. Am J Physiol Heart Circ Physiol, 2004, 287(3): H1369-H1377.
[38] KOLLIAS G, KONTOYIANNIS D. Role of TNF/TNFR in autoimmunity: Specific TNF receptor blockade may be advantageous to anti-TNF treatments[J]. Cytokine Growth Factor Rev, 2002, 13(4/5): 315-321.
[39] SIEGMUND D, KUMS J, EHRENSCHWENDER M, et al. Activation of TNFR2 sensitizes macrophages for TNFR1-mediated necroptosis[J]. Cell Death Dis, 2016, 7(9): e2375.
[40] CABAL-HIERRO L, LAZO P S. Signal transduction by tumor necrosis factor receptors[J]. Cell Signal, 2012, 24(6): 1297-1305.
[41] FAUSTMAN D, DAVIS M. TNF receptor 2 pathway: Drug target for autoimmune diseases[J]. Nat Rev Drug Discov, 2010, 9(6): 482-493.
[42] WILLIAMS R O, CLANCHY F I, HUANG Y S, et al. TNFR2 signalling in inflammatory diseases[J]. Best Pract Res Clin Rheumatol, 2024, 38(2): 101941.
[43] CACCI E, CLAASEN J H, KOKAIA Z. Microglia-derived tumor necrosis factor-alpha exaggerates death of newborn hippocampal progenitor cells *in vitro*[J]. J Neurosci Res, 2005, 80(6): 789-797.
[44] ROYALL J A, BERKOW R L, BECKMAN J S, et al. Tumor necrosis factor and interleukin 1 alpha increase vascular endothelial permeability[J]. Am J Physiol, 1989, 257(6 Pt 1): L399-L410.
[45] PAN W H, DING Y M, YU Y M, et al. Stroke upregulates TNFalpha transport across the blood-brain barrier[J]. Exp Neurol, 2006, 198(1): 222-233.
[46] PAN W, KASTIN A J. Increase in TNFalpha transport after SCI is specific for time, region, and type of lesion[J]. Exp Neurol, 2001, 170(2): 357-363.
[47] PAN W H, KASTIN A J. TNFalpha transport across the blood-brain barrier is abolished in receptor knockout mice[J]. Exp Neurol, 2002, 174(2): 193-200.
[48] QIN L Y, WU X F, BLOCK M L, et al. Systemic LPS causes chronic neuroinflammation and progressive neurodegeneration[J]. Glia, 2007, 55(5): 453-462.
[49] GOUWELEEUW L, POL C, SIMONIDES W S, et al. Evidence for neuroinflammation after myocardial infarction in a mouse model[J]. Heart Mind, 2017, 1(4): 134-140.
[50] VOET S, PRINZ M, VAN LOO G. Microglia in central nervous system inflammation and multiple sclerosis pathology[J]. Trends Mol Med, 2019, 25(2): 112-123.
[51] FOTIN-MLECZEK M, HENKLER F, SAMEL D, et al. Apoptotic crosstalk of TNF receptors: TNF-R2-induces depletion of TRAF2 and IAP proteins and accelerates TNF-R1-dependent activation of caspase-8[J]. J Cell Sci, 2002, 115(Pt 13): 2757-2770.
[52] RODRíGUEZ M, CABAL-HIERRO L, CARCEDO M T, et al. NF-kappaB signal triggering and termination by tumor necrosis factor receptor 2[J]. J Biol Chem, 2011, 286(26): 22814-22824.
[53] MOSS M L, JIN S L, MILLA M E, et al. Cloning of a disintegrin metalloproteinase that processes precursor tumour-necrosis factor-alpha[J]. Nature, 1997, 385(6618): 733-736.
[54] VAN HAUWERMEIREN F, VANDENBROUCKE R E, LIBERT C. Treatment of TNF mediated diseases by selective inhibition of soluble TNF or TNFR1[J]. Cytokine Growth Factor Rev, 2011, 22(5/6): 311-319.
[55] HARIDAS V, DARNAY B G, NATARAJAN K, et al. Overexpression of the p80 TNF receptor leads to TNF-dependent apoptosis, nuclear factor-kappa B activation, and c-Jun kinase activation[J]. J Immunol, 1998, 160(7): 3152-3162.
[56] HSU H, XIONG J, GOEDDEL D V. The TNF receptor 1-associated protein TRADD signals cell death and NF-kappa B activation[J]. Cell, 1995, 81(4): 495-504.
[57] HOU Y Y, WANG K, WAN W J, et al. Resveratrol provides neuroprotection by regulating the JAK2/STAT3/PI3K/AKT/mTOR pathway after stroke in rats[J]. Genes Dis, 2018, 5(3): 245-255.
[58] DONG J, XU X Q, ZHANG Q Y, et al. Critical implication of the PTEN/PI3K/AKT pathway during BMP2-induced heterotopic ossification[J]. Mol Med Rep, 2021, 23(4): 254.

(编辑:董宇　郭小燕)